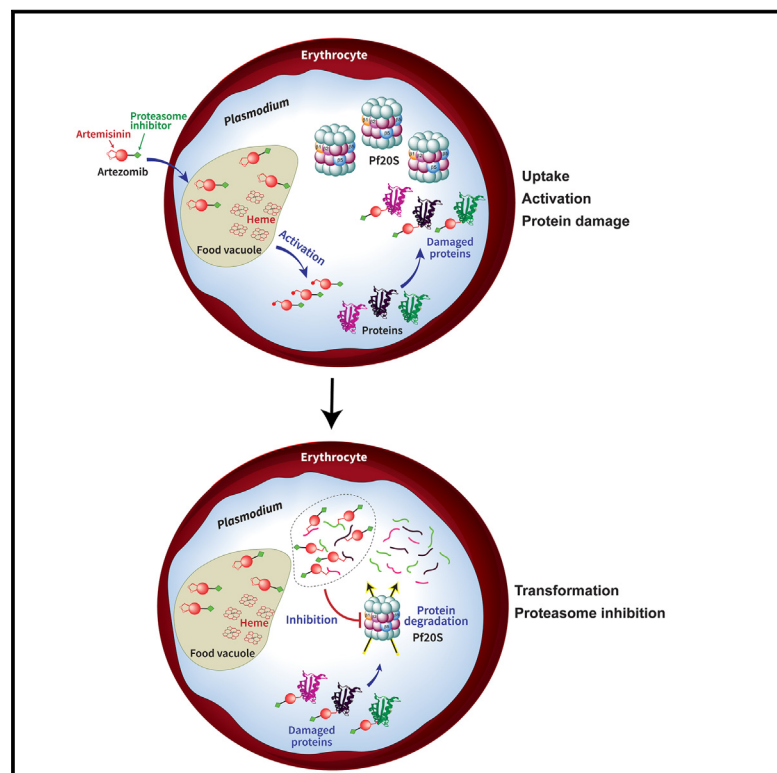# Cell Chemical Biology

Dual-pharmacophore artezomibs hijack the *Plasmodium* ubiquitin-proteasome system to kill malaria parasites while overcoming drug resistance

Graphical abstract

Authors

Wenhu Zhan, Daqiang Li,
Shubha Bevkal Subramanyaswamy, ...,
Carl F. Nathan, Laura A. Kirkman,
Gang Lin

Correspondence

lak9015@med.cornell.edu (L.A.K.),
gal2005@med.cornell.edu (G.L.)

In brief

Zhan et al. combined two anti-malarial agents—an artemisinin and a proteasome inhibitor—into a single compound called ATZ, which has an additional anti-malarial mechanism of action beyond that of its components. ATZ killed malaria resistant to either component or both.

Highlights

- ATZ links ART to an anti-malarial PI

- Malaria-activated ATZ installs the PI on parasite proteins

- ATZ overcomes resistance to both its components

- ATZ suppresses recrudescence of ART-resistant parasites in mice

CellPress

Article

Dual-pharmacophore artezomibs hijack the *Plasmodium* ubiquitin-proteasome system to kill malaria parasites while overcoming drug resistance

Wenhu Zhan,[1,8,9] Daqiang Li,[1,9] Shubha Bevkal Subramanyaswamy,[2] Yi Jing Liu,[2] Changmei Yang,[3] Hao Zhang,[1] Jacob C. Harris,[2] Rong Wang,[4] Songbiao Zhu,[3] Hedy Rocha,[5] Julian Sherman,[5] Junling Qin,[6] Mikayla Herring,[2] Nelson V. Simwela,[7] Andrew P. Waters,[7] George Sukenick,[4] Liwang Cui,[6] Ana Rodriguez,[5] Haiteng Deng,[3] Carl F. Nathan,[1] Laura A. Kirkman,[1,2,*] and Gang Lin[1,10,*]

[1]Department of Microbiology and Immunology, Weill Cornell Medicine, 1300 York Avenue, New York, NY 10065, USA
[2]Department of Medicine, Division of Infectious Diseases, 1300 York Avenue, New York, NY 10065, USA
[3]MOE Key Laboratory of Bioinformatics, Center for Synthetic and Systematic Biology, School of Life Sciences, Tsinghua University, Beijing 100084, China
[4]NMR Analytical Core Facility, Memorial Sloan Kettering Cancer Center, New York, NY 10065, USA
[5]Division of Parasitology, Department of Microbiology, New York University School of Medicine, New York, NY, USA
[6]Department of Internal Medicine, Morsani College of Medicine, University of South Florida, Tampa, FL, USA
[7]School of Infection and Immunity, Wellcome Centre for Integrative Parasitology, University of Glasgow, Glasgow, UK
[8]Present address: iCarbonX (Shenzhen) Co., Ltd., Shenzhen 518000, China
[9]These authors contributed equally
[10]Lead contact
*Correspondence: lak9015@med.cornell.edu (L.A.K.), gal2005@med.cornell.edu (G.L.)
https://doi.org/10.1016/j.chembiol.2023.04.006

SUMMARY

Artemisinins (ART) are critical anti-malarials and despite their use in combination therapy, ART-resistant *Plasmodium falciparum* is spreading globally. To counter ART resistance, we designed artezomibs (ATZs), molecules that link an ART with a proteasome inhibitor (PI) via a non-labile amide bond and hijack parasite's own ubiquitin-proteasome system to create novel anti-malarials *in situ*. Upon activation of the ART moiety, ATZs covalently attach to and damage multiple parasite proteins, marking them for proteasomal degradation. When damaged proteins enter the proteasome, their attached PIs inhibit protease function, potentiating the parasiticidal action of ART and overcoming ART resistance. Binding of the PI moiety to the proteasome active site is enhanced by distal interactions of the extended attached peptides, providing a mechanism to overcome PI resistance. ATZs have an extra mode of action beyond that of each component, thereby overcoming resistance to both components, while avoiding transient monotherapy seen when individual agents have disparate pharmacokinetic profiles.

INTRODUCTION

Artemisinin (ART) is currently the backbone of combination treatment for malaria, a protozoal infection responsible for 200 million cases and almost one-half of a million deaths each year.[1] ART is a pro-drug that it is activated by hemoglobin-derived ferrous heme or non-heme ferrous ions within the parasites.[2–4] Activation converts ART to radicals that cause extensive oxidative damage to lipids and proteins and lead to parasite death through multiple pathways.[2,5–9] These oxidized proteins overload the parasites' ubiquitin-proteasome degradation system (UPS), killing the parasite.[10] Increased cases of malaria recrudescence following ART monotherapy led to the use of ART-based combination therapy (ACT). However, ACT treatment failure is now widespread across Southeast Asia and has been associated with mutations in the protein Kelch13 (K13).

K13 mutations are now appearing in Africa and South America,[11–16] portending the potential spread of ART resistance in the regions of the world where the malaria burden is the most devastating. Additionally, pre-existing resistance to partner drugs in ACT accelerates the emergence and spread of ART resistance.[17] The higher the grade of partner drug resistance, the stronger the selection for ART resistance,[17] suggesting that even the combination of a proteasome inhibitor and an ART may not be sufficient to prevent the emergence of ART resistance. Novel approaches are needed to prevent a potential public health crisis in regions affected by malaria and spreading ART resistance. The hallmark of ART resistance is increased tolerance to ART at the early ring stage of the parasites' erythrocytic cycle. Multiple mechanisms of resistance have been associated with K13 polymorphisms,[18,19] including reduced ART activation arising from defects in hemoglobin catabolism that decrease the

abundance of free heme,[20] reduction in proteotoxic stress,[21] and prolongation of the ring stage of intra-erythrocytic *Pf* development,[22] ACT is additionally limited by the divergent pharmacokinetic profiles of the individual drugs; intermittent *de facto* monotherapy forfeits the intended synergistic effect against the emergence of ART resistance.[23]

Treatment of *Pf* with ART leads to accumulation of polyubiquitinated proteins that are delivered to the *Pf* proteasome (*Pf*20S) for degradation.[10] Killing of the malaria parasite by ART occurs when protein damage exceeds the capacity of the protein degradation machinery. *Pf* parasites are highly susceptible to proteasome inhibition at erythrocytic, liver, gametocyte, and gamete activation stages, suggesting that *Pf*20S has essential functions in all life cycle stages and making *Pf* 20S an appealing target for the development of anti-malarials.[24–32]

We and others have demonstrated that various classes of proteasome inhibitors (PI) can be designed to selectively target Pf20S over human proteasomes and that they are synergistic with ART.[25,32] The synergy may arise in part as ART treatment leads to accumulation of misfolded proteins with toxic effects and proteasome inhibition prevents the breakdown and removal of damaged proteins. As with other anti-malarials, *Pf* parasites can develop resistance to PIs, although this was demonstrated *in vitro* and required a high parasite inoculum compared with other compounds in development, suggesting a high *in vitro* barrier to resistance.[25,32] Moreover, in some cases, only a minor shift to an increased median effective concentration (EC$_{50}$) could be achieved.[24,25,32] However, Stokes et al.[25] reported that mutations conferring resistance to *Pf*20S inhibitors can be generated in K13 mutants, suggesting that there is no barrier to selection of PI resistance in parasites with pre-existing ART resistance mutations.

Given that PIs not only kill *Pf* on their own, but also make the parasites more susceptible to ART, we hypothesized that linking a PI with an ART analog through a non-labile tether could yield a hybrid compound with the ability to hijack the parasite UPS by creating a variety of protein-linked PIs *in situ*. It is well established that ART promiscuously and covalently attaches to proteins.[2,6] Thus, we reasoned that an ART-PI hybrid would yield ART-modified proteins whose proteasomal degradation products bearing a PI moiety could then inhibit the function of *Pf*20S by binding to its active proteolytic subunits. We propose that these hybrid compounds would have anti-parasitic activity beyond that of their individual moieties and only within the parasite be transformed into variable PIs with extended activity. With additional binding distal to the *Pf*20S active sites, the extended peptides of the PI-bearing degradation products would have a higher binding energy that could prevent the emergence of PI resistance and/or compensate for a loss of binding affinity caused by point mutations near the active sites that would otherwise decrease the efficacy of the PI. These peptides bearing a PI via an ART component could only be formed in parasites treated with the hybrid compounds and not when the two chemophores were administered separately.

Here we report combining the ART and PI moieties into one small molecule, termed an artezomib (ATZ), that overcomes resistance to its individual components and potentially prevents the emergence of resistance.

RESULTS

Design and biochemical activities of ATZs

We designed and synthesized an ATZ called ATZ4 (Figure 1A and Scheme S1), using an amide linker between a cyclic ether form of ART (ART1, Scheme S2) and PI01 (Scheme S1), a *Pf*20S inhibitor of a novel asparagine ethylenediamine class.[32,33] As a control, we synthesized deoxy-ATZ4, a compound whose ART moiety cannot be activated in the parasites because it lacks the endoperoxide of ART1 (Scheme S3). We coupled ART1 at the P4 position of PI01 because the S4 pocket of the *Pf*20S is partially exposed to solvent and we predicted that a bulky ART at this position would not interfere with the binding of the rest of the molecule to the active site of the *Pf*20S β5 subunit. This prediction was based on our experience with macrocyclic peptide Pf20S-selective inhibitors, where linking P2 and P4 maintained inhibitory activity against *Pf*20S.[34] Whereas ATZ4 was designed to be selective for the *Pf*20S proteasome over the human constitutive proteasome (hu c-20S) and human immunoproteasome (hu i-20S), we also synthesized ATZ2 (Figure 1A) that was also potent against hu-i20S. We needed to use ATZ2 as a tool compound for mechanistic studies where a large amount of purified proteasome is needed. Recombinant 28-meric eukaryotic proteasomes are not available, but native hu-i20S can be readily purified in quantity, in contrast with *Pf*20S.

As expected, ART1 itself was minimally active against *Pf*20S (IC$_{50}$ of 9,200 nM) and inactive against both human proteasomes (Figure 1B and Table 1). In contrast, PI01 was potent against *Pf*20S (IC$_{50}$ of 6.0 nM) and ~30- and 300-fold less active on hu i-20S and hu c-20S, respectively. ATZ2, ATZ4, and deoxy-ATZ4 were all active against Pf20S with a potency comparable with that of PI01. The relative activities of the ATZs for *Pf*20S versus human proteasomes mirrored the activities of their PI01 component. These results confirmed the prediction that the ART and deoxy-ART moieties of ATZs do not interfere with the binding of the PI to the monitored active sites of the respective proteasomes.

ATZs kill WT and PI-resistant strains of *Pf in vitro*

Next, we tested these compounds against *Pf* Dd2 wild type (Dd2^{WT}) and against Dd2β6^{A117D} and Dd2β5^{A49S}, two PI-resistant strains derived from Dd2 that harbor a mutation in the β6 subunit (A117D) or in the β5 subunit (A49S) of *Pf*20S, respectively (Figure 1B and Table 1).[24,32] As expected, the growth inhibitory activity of the ART analog ART1 was similar for Dd2 and Dd2β6^{A117D} and Dd2β5^{A49S} at comparable EC$_{50}$ values. Also as expected, Dd2β6^{A117D} and Dd2β5^{A49S} were 16- and >370-fold more resistant to PI01, respectively, than the parental strain Dd2. ATZ2/4 were 10 times more potent than ART1 and as potent as PI01 against Dd2 (Table 1). In contrast with PI01, growth inhibition of Dd2β6^{A117D} and Dd2β5^{A49S} by ATZ2/4 persisted with a ≤2.9-fold reduced potency for Dd2β6^{A117D} and ≤3.6-fold for Dd2β5^{A49S}, representing ≥5-fold and >100-fold improvement over PI01 against the respective strains. Without activable endoperoxide, deoxy-ATZ4 showed decreased activity against Dd2 compared with PI01, and much decreased activity against Dd2β6^{A117D} and Dd2β5^{A49S}. We reasoned that the anti-*Pf* activity of ATZs was not only derived from the ART moiety, but also from the PI moiety. Thus, ATZs substantially overcame the resistance to the PI moiety that was conferred by point mutations in *Pf*20S.
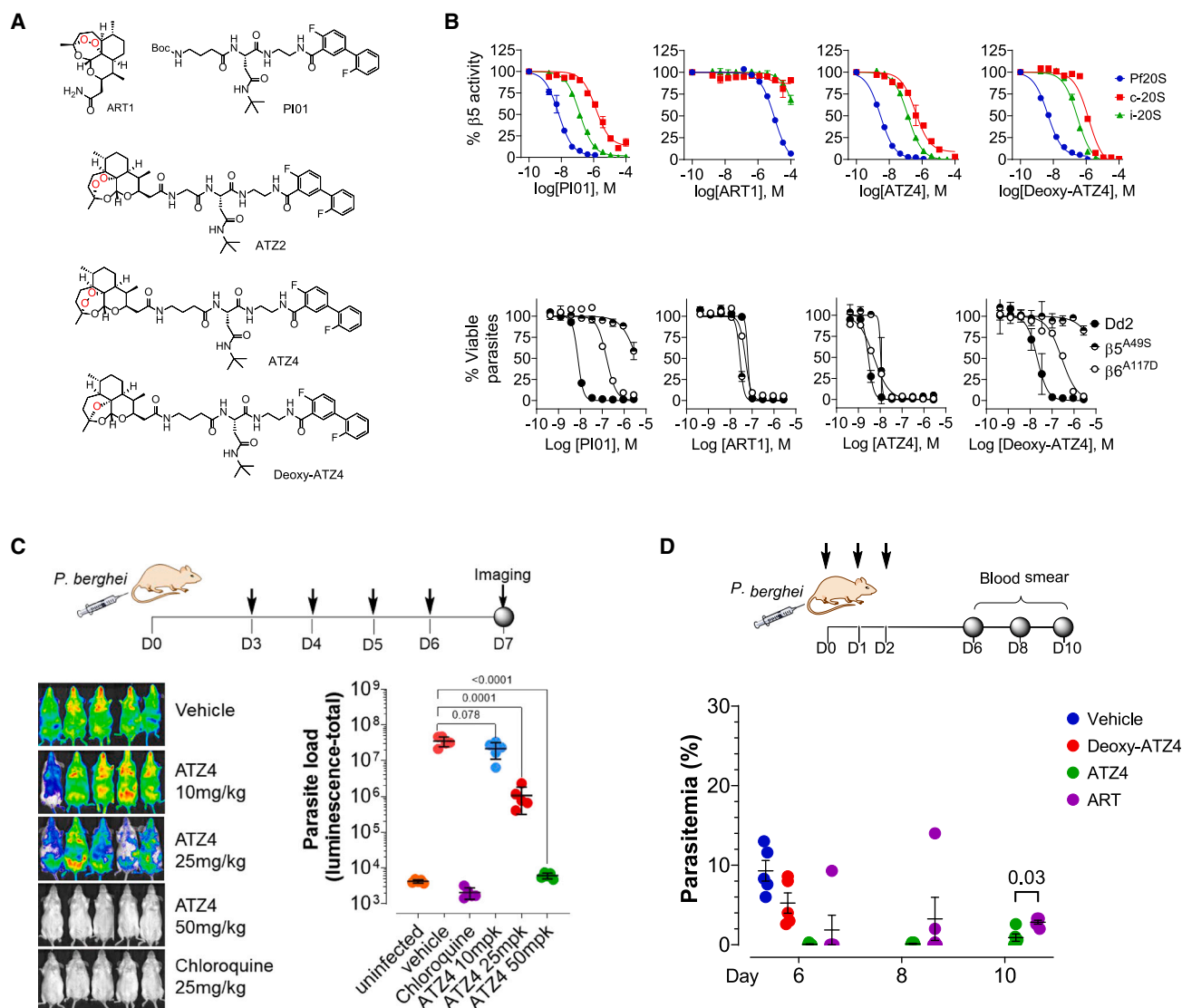
Figure 1. Design of hybrids of ART and PIs and their efficacy in parasite clearance and recrudescence

(A) Structures of ART analog ART1, PI01, and hybrid compounds.

(B) (Top) Dose-dependent inhibition of the proteasome activity and (bottom) inhibition of the *Plasmodium* parasite growth in red blood cells. Dd2β6[A117D] and Dd2β5A48S are mutant strains resistant to PIs.

(C) *In vivo* efficacy of ATZ4 against *P. berghei* ANKA lux in mice. (Top) Scheme of the *in vivo* efficacy study with Swiss Webster mice (5 per treatment). *P. berghei* ANKA lux was injected in the tail vein on day 0. ATZ4 was administered interaperitoneally at 10, 25, or 50 mg/kg on day 3 to day 6 once daily for a total of four doses. Chloroquine was used as a positive control at 20 mg/kg intraperitoneally. Bioluminescence in each mouse was recorded on day 7. (Left) Luminescence images of mice in respective treatment groups. (Right) Quantification of parasite load in luminescence in each group in (left). The experiment was performed twice, and a representative is shown. Error bars represent standard deviations of the mean.

(D) *In vivo* efficacy of ATZ4 against recrudescence of *P. berghei* K13[R551T]. (Top) Scheme of the modified Peters' 4-day suppressive test.[35] Mice infected with *Pb* ART-resistant K13[R551T] mutant were treated with vehicle, ART (50 mg/kg), ATZ4 (100 mg/kg), and deoxy-ATZ4 (100 mg/kg) administered via interaperitoneal injection 3 h after inoculation of parasites on day 0 and continued on day 1 and day 2 (shown by arrows). Parasitemia in each mouse was monitored by microscopic analysis of Giemsa-stained blood smears on days 6, 8, and 10. The rates of recrudescence in each cohort on the indicated days were plotted as the percentages of mice with a positive smear. Error bars represent standard deviations of the mean.

ATZ4 clears *Plasmodium berghei* infection and suppresses recrudescence in mice

To learn if an ATZ possessed *in vivo* efficacy, we infected mice with the rodent parasite *P. berghei* ANKA Lux on day 0 and started once-daily treatment on day 3 for 4 days (Figure 1C). Parasite loads were quantified by luminescence on day 7. As

expected, the anti-malarial agent chloroquine at 20 mg/kg reduced the parasite load below the limit of detection. Although the PI moiety of ATZ4 was designed to inhibit the *Pf*20S, not the *P. berghei* 20S, ATZ4 demonstrated dose-dependent therapeutic effects in the mouse model. There was no detectable effect at 10 mg/kg, a 1.2 $\log_{10}$ decrease in parasite load at

Table 1. Proteasome inhibition activity and *Plasmodium* growth inhibition of ATZs and their constituent pharmacophores

	IC$_{50}$ (nM)			EC$_{50}$ (nM)			
ID	*Pf*20S	Hu i-20S	Hu c-20S	*Pf* Dd2^{WT}	Dd2β6^{A117D}	Dd2β5^{A49S}	HepG2
ART1	9,200 ± 720	>100,000	>100,000	43.7 ± 12.7	27.9 ± 11.0	30.2 ± 2.6	>100,000
PI01	6.0 ± 0.8	200 ± 46	2,000 ± 240	7.4 ± 0.2	121 ± 20	>2,770	>100,000
ATZ2	2.9 ± 0.6	73 ± 19	210 ± 40	3.0 ± 0.6	4.4 ± 1.1	10.9 ± 2.6	5,800 ± 620
ATZ4	4.3 ± 0.9	200 ± 57	890 ± 140	4.3 ± 1.3	6.7 ± 2.2	5.9 ± 1.9	9,400 ± 1,700
Deoxy-ATZ4	4.4 ± 0.5	300 ± 22	1100 ± 46	21.6 ± 1.4	246.0 ± 44.5	>2,770	10,800 ± 500

All data are means of at least three independent experiments and are presented with standard deviation. Data were rounded to three or fewer significant figures.

25 mg/kg, and a >3 log$_{10}$ decrease at 50 mg/kg, to below the limit of detection.

The *in vivo* efficacy of ATZ4 enabled us to ask if ATZ4 could suppress the recrudescence of *P. berghei* bearing mutations in K13 proteins. We also asked whether the efficacy of ATZ4 should be attributed to the ART moiety, the PI moiety, or both. To address this question, we used an established mouse model of recrudescence based on an engineered *P. berghei* strain called G2025 ^{R551T} that bears the K13 mutation K13^{R551T} and mimics the recrudescence phenotype of the equivalent *Pf* K13 mutant, K13^{R539T}.[35] We infected mice intravenously with mouse red blood cells infected (^{i}RBC) with WT *P. berghei* (1.6 × 10^5 ^{i}RBC) or with G2025^{R551T} (10^6 ^{i}RBC) and initiated treatment 3 h after inoculation and once daily for 2 more days (Figure 1D). Test compounds were administered by interaperitoneal injection, giving ART at 50 mg/kg and ATZ4 or deoxy-ATZ4 at 100 or 120 mg/kg (Figure S1A). Both ART and ATZ4 completely suppressed WT *P. berghei* for up to 16 days of follow-up (Figure S1B), whereas the cohorts treated with vehicle or deoxy-ATZ4 showed positive smears by day 6. In mice inoculated with G2025^{R551T}, all mice in the vehicle- and deoxy-ATZ4-treated groups showed positive smears by day 6. Of the mice treated with ART, 20% showed a positive blood smear on day 6, 40% on day 8, and 100% on day 10. In contrast, of mice treated with ATZ4, 0%, 0%, and 60% were smear positive on days 6, 8, and 10, respectively. Given that deoxy-ATZ4 was ineffective in suppressing the growth of both WT and G2025^{R551T} *P. berghei*, we hypothesized that ATZ4 was better able than ART to suppress recrudescence of the ART resistant parasites because of ATZ4s intra-parasitic transformation to more effective PIs.

Activation of ATZ produces PIs in a model system

To gain insight into the modes of action of ATZs, we devised a model system to test the hypothesis that degradation products of a protein covalently attached to an ATZ can inhibit a proteasome (Figure 2A). Because of the limited supply of purified *Pf*20S, we used human i-20S instead and β-casein as a substrate, as it is an intrinsically unstructured protein that can be degraded by i-20S and its PA28α regulator without ubiquitination. Hemin and ascorbate constituted an ART activating system to model conditions in the parasite where Fe^{2+}-heme activates the endoperoxide in ART,[2] leading to a carbon-centered ART radical that attaches covalently to proteins. β-Casein was incubated with hemin and ascorbate in the presence of PI01, ART1, or the potent i-20S inhibitor ATZ2 in two identical groups.

After 4 h at 25°C, one group of samples was dialyzed to remove small molecules while retaining proteins; the other group was not dialyzed. All samples were then incubated with i-20S/PA28α and aliquots removed at intervals to analyze β-casein degradation (Figure 2B). In the dialyzed set, prior exposure of β-casein to ATZ2 led to marked inhibition of the degradation of β-casein despite any free ATZ2 having been dialyzed out of the reaction mixture before addition of the proteasome. In contrast, exposure of β-casein to PI01 or ART1 followed by dialysis allowed the unimpeded degradation of β-casein by i-20S/PA28α (Figure 2B, left). In the non-dialyzed control samples, PI01, ART1, and ATZ2 were all present when i-20S and PA28α were added, and PI01 and ATZ2 inhibited the degradation of β-casein, whereas ART1 did not (Figure 2B, right). Thus, incubation of β-casein with activated ATZ2, but not with activated ART1, generated new, non-dialyzable PIs that inhibited i-20S from hydrolyzing β-casein.

The non-dialyzable PIs were presumably β-casein peptides decorated with the PI moiety of ATZ2 by the covalent attachment of its ART moiety. We confirmed this by proteomic analyses of PI01-, ART1-, and ATZ2-treated β-casein (Scheme S4 and Table S1). We unambiguously identified the peptide SLVYPFPGP^{80} from ATZ2 treated β-casein, in which proline-80 was modified by ATZ2 (Figure 2C and Table S2) and the peptide F^{67}AQTQSL-VYPFPGPIPN from ART1 treated β-casein, wherein phenylalanine-67 was modified by ART1 (Figure 2D and Table S3). As expected, no modified β-casein peptides were identified after incubation with PI01. These results suggest that degradation of an ART-damaged protein by the proteasome was not affected by covalent modification with ART, yet ATZ2, as a PI-coupled ART, converted β-casein and/or its degradation products to PIs. Because ARTs modify numerous proteins in *Pf*, treatment of *Pf* with an ATZ would presumably convert many *Pf* proteins into new PIs with variable extended peptides, including in PI-resistant parasite strains.

ATZs overcome resistance of *Pf* to ARTs

The majority of malaria resistance to ART are associated with mutations in PfK13 and are not manifest as a shift in the EC$_{50}$ in the standard 72-h assay, but rather a relative resistance seen only in the early ring stage of the erythrocytic cycle. To test if ATZs can circumvent the ART resistance conferred by K13 polymorphism, we conducted a ring-stage survival assay (RSA) with *Pf* strains Cam3.I^{rev} and Cam3.I^{R539T}. The latter strain is a field isolate with a K13 polymorphism associated with ART resistance, whereas Cam3.I^{rev} is an ART sensitive revertant
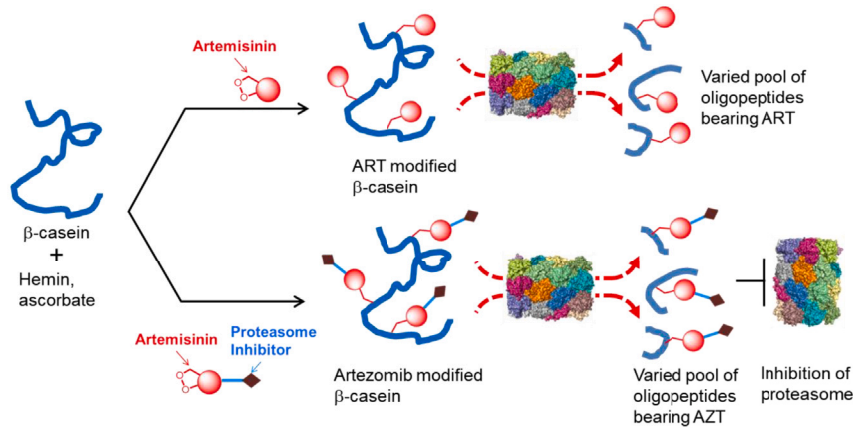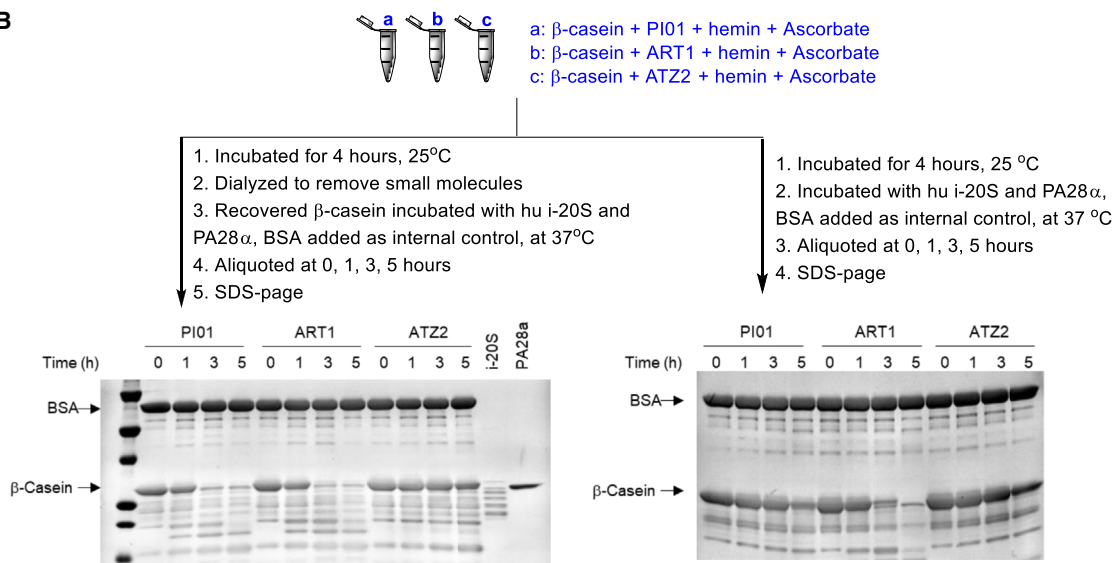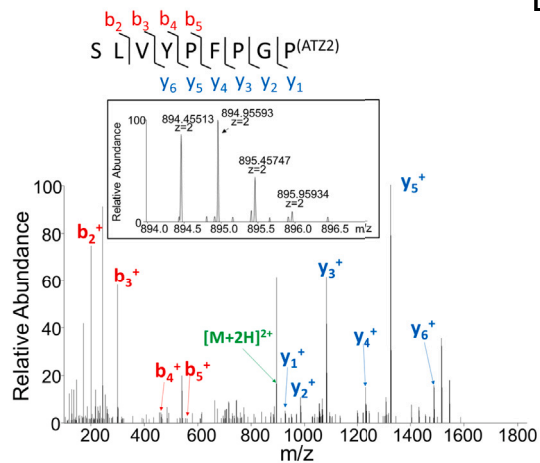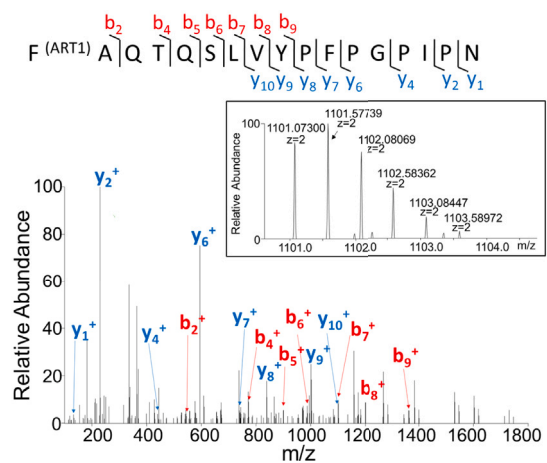
(legend on next page)

where the mutant K13 was genetically modified back to the WT K13.[18] Highly synchronized 0- to 3-h ring stage parasites were treated with the DMSO vehicle alone, dihydroartemisinin (DHA), ART1, PI01, or ATZ4 at the indicated concentrations for 6 h (Figure 3A). We then washed off the compounds and maintained the parasite cultures at 37°C for a further 66 h. Live parasites were analyzed by flow cytometry and survival expressed relative to that in the DMSO control. As expected, compared with Cam3.I^{rev}, Cam3.I^{R539T} was highly resistant to DHA and slightly resistant to ART1 (Figure 3B), whereas Cam3.I^{R539T} was as susceptible as Cam3.I^{rev} to ATZ4. Interestingly, Cam3.I^{R539T} was more sensitive than Cam3.I^{rev} to the PI01. These data confirmed that ATZs can circumvent ART resistance associated with K13 mutation at early ring stages.

Extended RSAs have been proposed to better reflect clinical efficacy.[36] Accordingly, we performed an extended RSA by pulsing parasites as in the standard RSA and then monitoring parasite growth over 7 days. As expected, parasites pulse-treated with DHA, PI01, or ART1 re-established normal growth. In contrast, parasites of both the ART-sensitive and ART-resistant lines that had been treated with ATZs had significantly lower parasitemia on day 7 (Figure 3C), indicative of prolonged growth inhibition.

Recently, parasite lines were generated that demonstrate a shift to a higher EC$_{50}$ to ART. These parasite lines were derived by exposing Dd2 to daily DHA for a prolonged period of time (J.Q. and L.C., unpublished data). Using a standard 72-h in vitro assay, we compared the susceptibilities of these DHA-resistant clones to the test compounds. These clones were highly resistant to DHA, modestly resistant to ART1, and equally susceptible to ATZ4 and deoxy-ATZ4 as the WT Dd2 (Figure 3D). Thus, ATZ4 could reverse resistance in recently created lines notable for having a shift in EC$_{50}$ parasite lines, most likely because of the potency of the PI component.

PI-resistance mutations decrease binding affinity of non-activated ATZs to Pf20S

Several studies reported that mutations in Pf20S, such as β6^{A117D}, β6^{A117V}, β6^{A208L}, β5^{A20S}, and β5^{A49S}, confer resistance to PIs.[24,25,32] All of these amino acids are involved in the binding of PIs to the Pf20S β5 and their mutation reduces PI binding with a concurrent shift to a higher EC$_{50}$.[24,32,35] Pf strains bearing Pf20S β5^{A49S} and β6^{A117D} mutations were highly resistant to PI01, but not to ATZs in cell-based assays (Tables 1 and S2). To relate growth inhibition to the pharmacodynamic effect, we used a probe compound, MV151, that covalently and irreversibly binds to proteasome active sites[37] and asked if pretreatment of Pf20S with our compounds blocks the binding of MV151. As ex-

pected, 1 h incubation of lysate of Dd2^{WT} with either PI01 or ATZ4 dose dependently blocked labeling of β5 by subsequently added MV151 (Figure 4). Under the same conditions, the β6^{A117D} and β5^{A49S} mutations prevented PI01 and ATZ4 from inhibiting MV151's labeling of β5 of the Pf20Sβ6^{A117D} and Pf20Sβ5^{A49S} in lysates derived from the PI-resistant parasite lines (Figures 4 and S3). This indicates that these mutations reduced the binding affinity of PI01 and ATZ4 to Pf20S β5 as was shown for other PIs when testing resistant parasite lysate.[32]
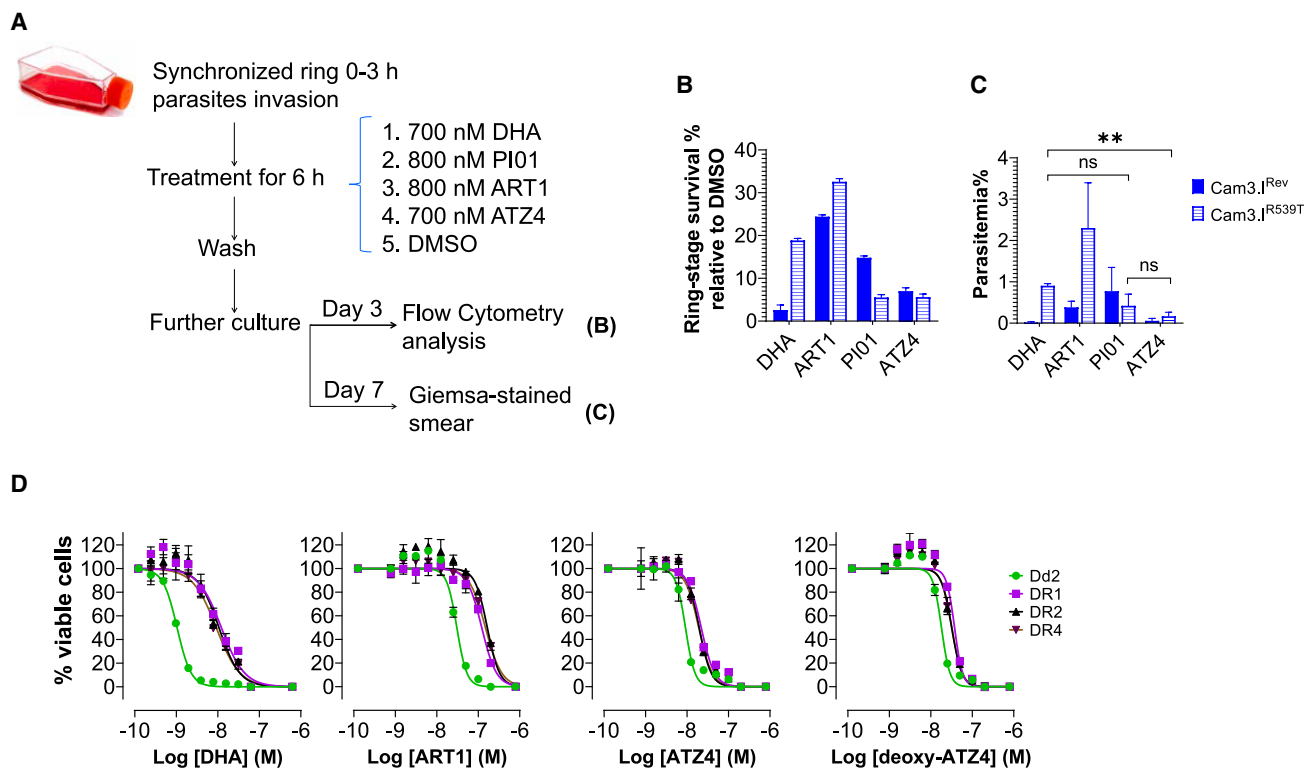
Activation of ATZs overcomes resistance of Pf to PIs

The seemingly contradictory results between the growth inhibition potency of ATZ4 against the Dd2^{WT}, Dd2β5^{A49S}, and Dd2β6^{A117D} strains (Tables 1 and S2) and the enzyme labeling in Pf lysates (Figure 4) could be explained if ATZs are converted only by live parasites, but not by their cell-free lysates, into new PIs that are active against both WT and PI-resistant parasites. To confirm that ATZs were indeed activated inside the parasites, we designed and synthesized ATZ-P1, a probe with a clickable azido group, and its direct comparator deoxy-ATZ-P1 (Figure 5A and Scheme S5). Both compounds were highly potent inhibitors of Pf20S β5 and of Pf growth (Figure 5A). We treated Pf Dd2 with 700 nM ATZ-P1, deoxy-ATZ-P1 or ART for 6 h (Figure 5B). We then washed off excess compounds, lysed the parasites, and reacted equal amounts of their soluble proteins with fluorescent Cy3-alkyne in the presence of copper (I). Labeled proteins and peptides were resolved on a tricine SDS-PAGE gel, followed by in-gel fluorescence visualization. There was minimal labeling of proteins and peptides in samples treated with deoxy-ATZ-P1 or ART (Figure 5B). In contrast, ATZ-P1 led to substantial labeling of proteins and peptides, indicating that ATZ-P1 was activated within Pf and covalently attached to diverse proteins.

To then confirm that the parasite proteasomes were inhibited after the activation of the endoperoxide in ATZ, we pulse-treated late-stage Dd2^{WT}, Dd2β6^{A117D}, and Dd2β5^{A49S} parasites with DMSO as a vehicle control, DHA (700 nM), PI01 (800 nM), ART1 (800 nM), a 1:1 combination of PI01 (800 nM) and ART1 (800 nM), ATZ4 (700 nM), or deoxy-ATZ4 (700 nM) for 6 h. After thoroughly washing off the compounds and recovering the parasites from the red blood cells, we lysed the parasites and labeled Pf20S with MV151 (Figure 5C). The labeling of Pf20S by MV151 in lysates from parasites treated with DHA, PI01, ART1, the combination of PI01 and ART1, and deoxy-ATZ4 was similar to the labeling of Pf20S β5 in DMSO-treated samples, confirming that the Pf20S in each sample was not inhibited. When the washing steps were omitted, PI01 and ATZ4 blocked the labeling of Pf20S β5 by MV151 (Figure S2), confirming that both of these compounds could enter red bloods cells and the

---

Figure 2. Mode of action of ATZ in the degradation of β-casein by 20S

(A) Illustration of degradation of β-casein by human i-20S after incubation with ART or ATZ activated by hemin and ascorbate.

(B) Degradation of β-casein. β-Casein was treated under indicated conditions (a, b, or c). (Left) after dialysis to remove the inhibitors, hemin and ascorbate, the treated β-casein was incubated with i-20S and PA28α with bovine serum albumin as an internal control. Aliquots were taken at indicated times and samples run on SDS-PAGE and stained with Coomassie blue. (Right) Without dialysis, aliquots were taken from each reaction at indicated time points and samples run on SDS-PAGE and stained with Coomassie blue. Representative images of three independent experiments for dialysis and two for non-dialysis.

(C) The tandem mass spectrometry (MS/MS) spectrum of the ATZ2-modified peptide SLVYPFPGP80. The inserted mono-isotope peak at m/z 894.45557 matches the theoretical mass of the aforementioned peptide modified by ATZ2. This peptide was not observed in PI01 treated or in ART1-treated β-casein samples through manual check.

(D) The MS/MS spectrum of the ART1 modified peptide F67AQTQSLVYPFPGPIPN. The inserted mono-isotope peak at m/z 1101.07361 matches the mass of the aforementioned peptide modified by ART1. This peptide was not observed in PI01 treated nor in ATZ2-treated β-casein samples through manual check.

A

Synchronized ring 0-3 h
parasites invasion

Treatment for 6 h
1. 700 nM DHA
2. 800 nM PI01
3. 800 nM ART1
4. 700 nM ATZ4
5. DMSO

Wash

Further culture
Day 3 → Flow Cytometry analysis **(B)**
Day 7 → Giemsa-stained smear **(C)**

B

C

D

Figure 3. ATZs overcome ART resistance

(A–C) Effects of compounds in RSA.

(A) Red blood cells infected with highly synchronized ring-stage parasites were treated with DMSO, DHA, ART1, PI01, or ATZ4 at indicated concentrations. After 6 h the compounds were washed off.

(B) The parasite cultures were allowed to grow for 66 h. Viable parasites were analyzed by flow cytometry and their numbers normalized to values for the DMSO control.

(C) Aliquots of parasites from (A) were cultured for a further 96 h. Parasitemia was quantified by Giemsa-stained smears. Error bars in (B and C) represent standard deviations of the mean. p values of unpaired two-tailed t-tests in (C) between DHA and ATZ4 groups, DHA and PI01 groups, and PI01 and ATZ4 groups were performed in GraphPad Prism (version 9.4.0). $**p < 0.005$. ns, not significant.

(D) ATZ4 and deoxy-ATZ4 overcome ART-resistance at trophozoite-stage. DR1, DR2, and DR4 are DHA-resistant clones derived from the Dd2 strain that were selected *in vitro*. Graphs are representative of two independent experiments.

parasites within them. Despite the extensive washing, *Pf*20S in the lysate from the parasites treated with ATZ4 showed substantial inhibition of labeling of *Pf*20S β5 by MV151 (Figure 5D). Moreover, this activity was similarly effective against intracellular *Pf*20S β5 with the $β6^{A117D}$ and $β5^{A49S}$ mutations (Figure 5D), in contrast with the minimal inhibition of *Pf*20S $β6^{A117D}$ and $β5^{A49S}$ labeling by ATZ4 itself (Figure 4). These results are in contrast with experiments with parasite lysates and consistent with transformation of ATZ4 within live parasites to persistently retained intracellular moieties capable of sustained inhibition of *Pf*20S β5.

ATZs overcome dual resistance of *Pf* to ART and PIs

To test the likelihood that ATZs might markedly decrease the emergence of resistance to either component of the hybrid molecule, we tested the growth inhibitory activity of ATZs against a *Pf* strain with a mutation conferring resistance to ART and an additional mutation conferring resistance to PIs. To do so, we engineered the $K13^{R539T}$ mutation into the PI-resistant strain $Dd2β6^{A117D}$, creating the double mutant strain $Dd2β6^{A117D}K13^{R539T}$ (Figures 6A and S4). ATZ4 was equipotent against

Dd2, $Dd2β6^{A117D}$, $Dd2K13^{R539T}$, and $Dd2β6^{A117D}K13^{R539T}$. In contrast, deoxy-ATZ4 was 5.6- and 11.0-fold less potent against $Dd2β6^{A117D}$ and $Dd2β6^{A117D}K13^{R539T}$, respectively, compared with Dd2 and $Dd2K13^{R539T}$. Thus, ATZs can overcome resistance to each of their constituent pharmacophores in a strain that bears resistance to both.

DISCUSSION

The malaria proteasome is an attractive target for drug development because its pharmacological inhibition is detrimental to the viability of the parasite at multiple stages of its life cycle. Additionally, synergistic effects have been reported for ART with *Pf*20S inhibitors, irrespective of whether they inhibit the β2 or β5 subunits.[29,32,34,38,39] However, the reported development of dual resistance through mutations in β5 or β2 in ART-resistant Pf Cam3.II C580Y[38] suggests that a *Pf*20S inhibitor drug could drive the emergence of parasites with dual resistance to ART and the PI, if the PI were used as monotherapy. A recent study of mutations in Pf20S in clinical isolates demonstrated no resistance to the PIs tested in the study.[40] However, there remains a
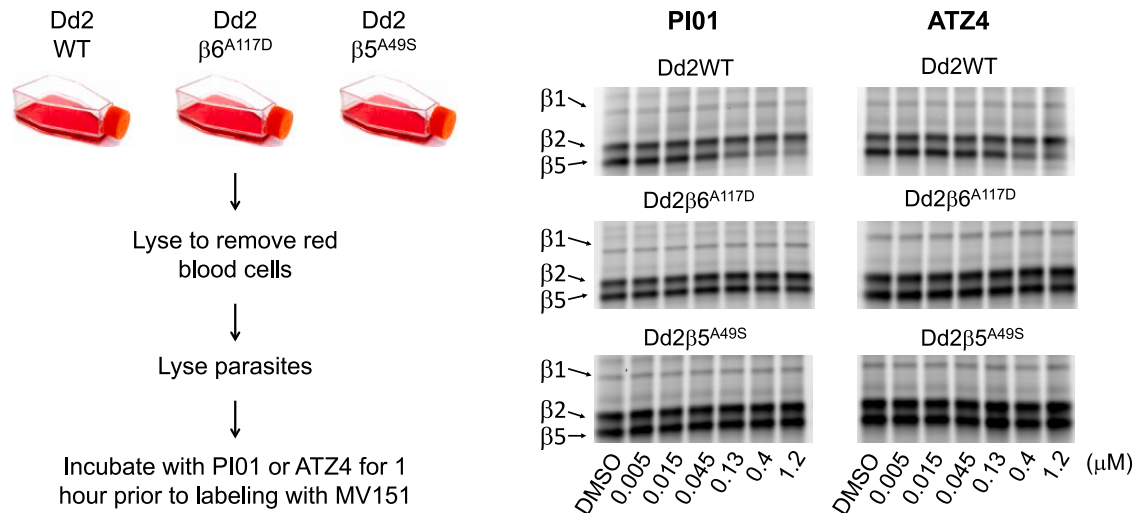
Figure 4. Inhibition of Pf20S, Pf20Sβ6^{A117D}, and Pf20Sβ5^{A49S} by PI01 or ATZ4 in lysates of Dd2^{WT}, Dd2β6^{A117D}, and Dd2β5^{A49S} parasites

This was assessed by the compounds' ability to block labeling of the parasites' proteasomes by the activity-based fluorescent probe MV151 after a 1-h preincubation.

risk that ART resistance may develop in clinical isolates harboring mutations that could confer resistance to PIs. A combination of a PI and an ART administered as separate agents may not suffice to combat the evolution of resistance to either or both. In this study, we proposed and confirmed an approach that takes advantage of the broad covalent reactivity of intra-parasite-activated ARTs to force the parasites to generate novel PIs in situ. This should impose a high barrier against the emergence of such resistance, for two reasons.

First, the conjugation of a PI with an ART analog confers on the resulting ATZs an additional mechanism of action, distinct from the mechanisms of the individual pharmacophores. This new mechanism of action allows ATZs to overcome resistance to the PI moiety. We confirmed that ATZs retain both proteasome inhibitory activity and the reactive alkylating activity of ART. The ability to overcome resistance conferred by point mutations in Pf20S is associated with ATZ-dependent formation of proteasome-inhibitory activity that is not removed from the parasites by washing procedures that remove ATZ itself. We ascribe this more robust proteasome inhibitory activity to the demonstrable formation of proteasomal degradation products of ATZ-damaged proteins. The oligopeptides to which the ART-derived radicals are attached seem to stabilize the presentation of the PI moiety of the ATZ at the Pf20S active site, compensating for the decreased binding affinity conferred by the point mutations. In short, with the malaria parasite's dependence on the proteasome to remove ART-damaged proteins, ATZs hijack the parasite protein degradation machinery to create a pool of PI-containing oligopeptides that remain effective against parasites with mutations in the Pf20S subunits that may confer resistance to the unmodified PI. Moreover, the PI moiety of ATZs continues to synergize with their ART moiety, as seen when Pf is jointly treated with PIs and ARTs as separate agents.[29,32,34,38,39]

Second, because the actions of ART and the improved action of the PI are delivered by a single molecule, a single pharmacokinetic profile will preclude temporary exposure to only one of the components in the two-pharmacophore combination. Tempo-

rary monotherapy is a risk of combination chemotherapy with separate agents that have disparate pharmacokinetics.

Microbial infection and host resistance involve ongoing evolutionary point and counterpoint. With few exceptions, the introduction of novel anti-microbials is followed by the emergence of resistant pathogens, especially when numbers of pathogenic microbes reach high levels. For example, there are more than 10^{12} Plasmodium parasites in an active malaria patient, so that even with some of the drugs in development showing no detection of resistance in a culture of 10^9 parasites, the emergence of resistance is practically inevitable.[41,42] Thus, there is great concern that we will run out of new pathogen drug targets for selective inhibition. The problem is further aggravated when both host and pathogen are eukaryotes, putting a premium on our ability to take advantage of subtle differences in conserved pathways and structures. Anti-microbial agents having selectivity for the pathogen over homologous host structures are becoming an important part of the anti-infective armamentarium.[43] In this work, we exploited the development of PIs with a high degree of selectivity for the pathogen over the host, an effort whose feasibility was introduced with studies on Mycobacterium tuberculosis.[44] Further, we have exploited the pathogen's reliance on hemoglobin digestion during the erythrocytic stage of its life cycle, which leads to a buildup of heme residues whose redox chemistry activates ART. ATZs exploit the activation of ART to trick the pathogen into generating a plethora of PIs from its own proteins. The resulting pool of PIs that are retained inside the parasites gain binding energy through their oligopeptide handles, overcoming resistance conferred by Pf20S mutations. Moreover, via their PI components, ATZs will be active against the parasites at stages of their life cycle when they contain less heme than at erythrocytic stages.

ART resistance is now established in Southeast Asia and complicated by the concomitant spread of resistance to partner drugs in ACTs.[13,45–51] In light of these concerns, triple ART-based combination therapies have been proposed and a clinical trial was conducted to prevent the emergence of resistance to
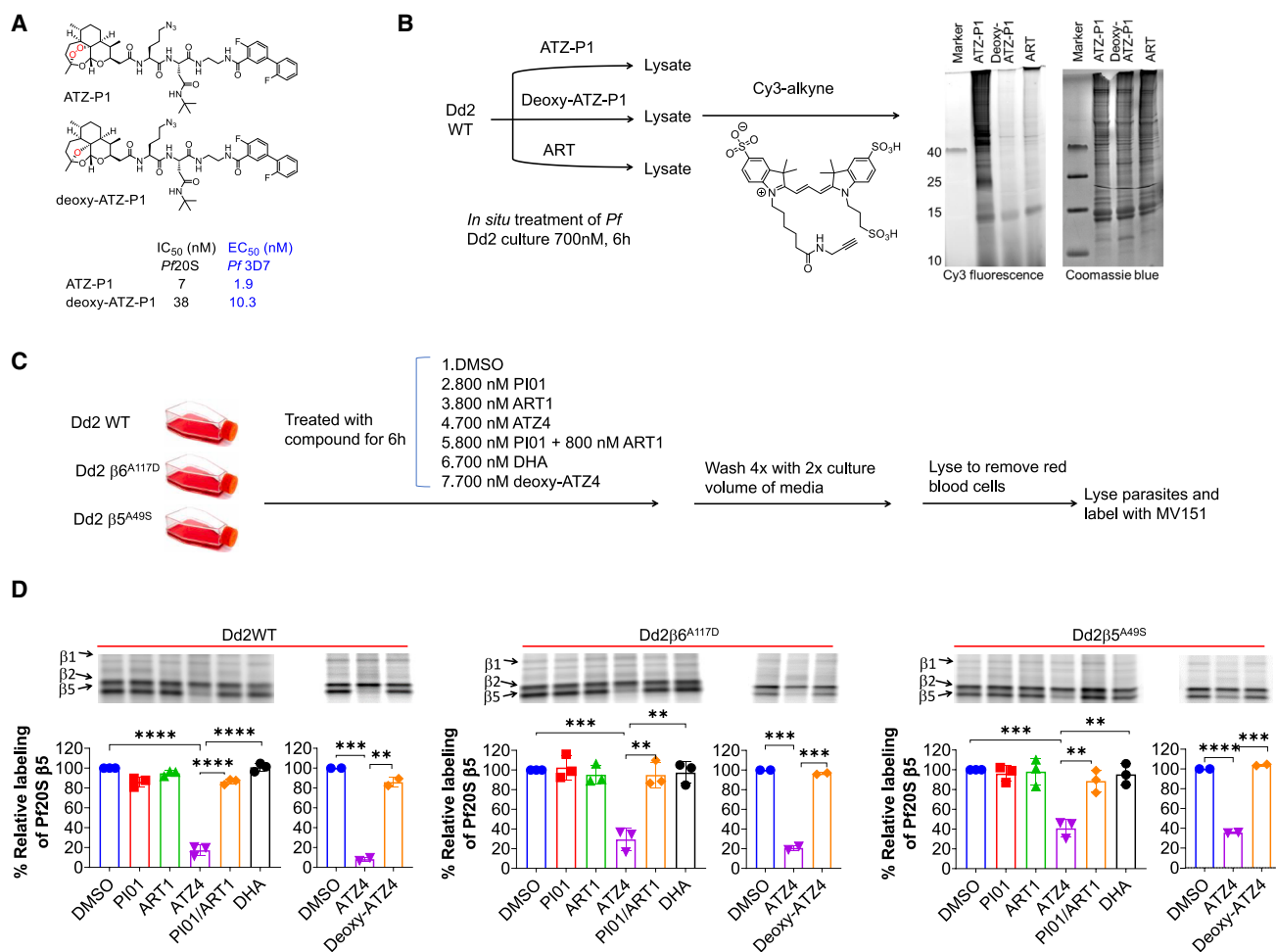
Figure 5. Mode of action of ATZ in *P. falciparum*

(A) Structures of ATZ-P1 and deoxy-ATZ-P1 and their enzyme inhibition and parasite growth inhibition activities.

(B) *Pf* Dd2 parasites were treated with ATZ-P1, deoxy-ATZ-P1, and ART at 700 nM for 6 h. Equal amounts of the parasite lysates were reacted with Cy3-alkyne for 1 h and resolved on an SDS-PAGE gel. Fluorescence signals were recorded on a fluorescence scanner (left) and the loading control was shown by Coomassie blue (right).

(C) Scheme of experiment design. Parasites were treated with DMSO, PI01, WZ1840, ATZ4, PI01/ART1 (1:1), DHA, or deoxy-ATZ4 at indicated concentrations for 6 h and compounds were then washed off before hypotonic lysis of red blood cells. Parasites were then lysed and labeled with MV151.

(D) Fluorescent scanning images of representative SDS-PAGE gels of *Pf*20S labeling by MV151 of samples in (C). Quantification of labeling was performed with ImageJ. Percentages of labeling inhibition were calculated by normalizing the ratios of density of β2/β5 bands to that of DMSO treated. Data are means ± standard error of two or three independent experiments. p values of unpaired two-tailed t-tests between the DMSO and ATZ4 groups, ATZ4 and PI01/ART1 groups, and ATZ4 and deoxy-ATZ4 groups were performed in GraphPad Prism (version 9.4.0). $**p < 0.005$, $***p < 0.0005$ and $****p < 0.0001$.

the partner drugs in ART-resistant *Pf*.[52] The parasites' ability to develop drug resistance highlights concerns about the eventual failure of these key anti-malarials and the potential failure of any new anti-malarial drugs under development.[11,12] Our findings that ATZs can overcome ART resistance conferred by K13 mutations, PI resistance conferred by mutations in proteasome subunits, and dual resistance conferred by both mutations in a single *Pf* line give hope that such a compound could greatly hinder the emergence of resistance to ART and to itself.

Limitations of the study

This study offers a proof of concept to build on to develop clinically relevant anti-malarials with a novel mechanism of action. However, we only demonstrated *in vivo* efficacy in mouse models using a rodent malaria, and our ATZs were not optimized for the *Pb*20S active sites. Moreover, while no mouse toxicity was observed, ATZs require optimization for oral bioavailability and other pharmacological properties as well as formal evaluation for potential toxicities. Given the difficulty in obtaining *Pf*20S in sufficient quantity and purity and in a native confirmation, we used a heterologous proteasome for *in vitro* studies. Only a subset of the ATZ-bearing peptides created upon activation are likely to be effective inhibitors of Pf20S, and further work is needed to characterize them and their mechanism of action. Finally, while *de novo* resistance to ATZs is unlikely to arise through the joint acquisition of mutations in Kelch and the proteasome, resistance might arise through other means.
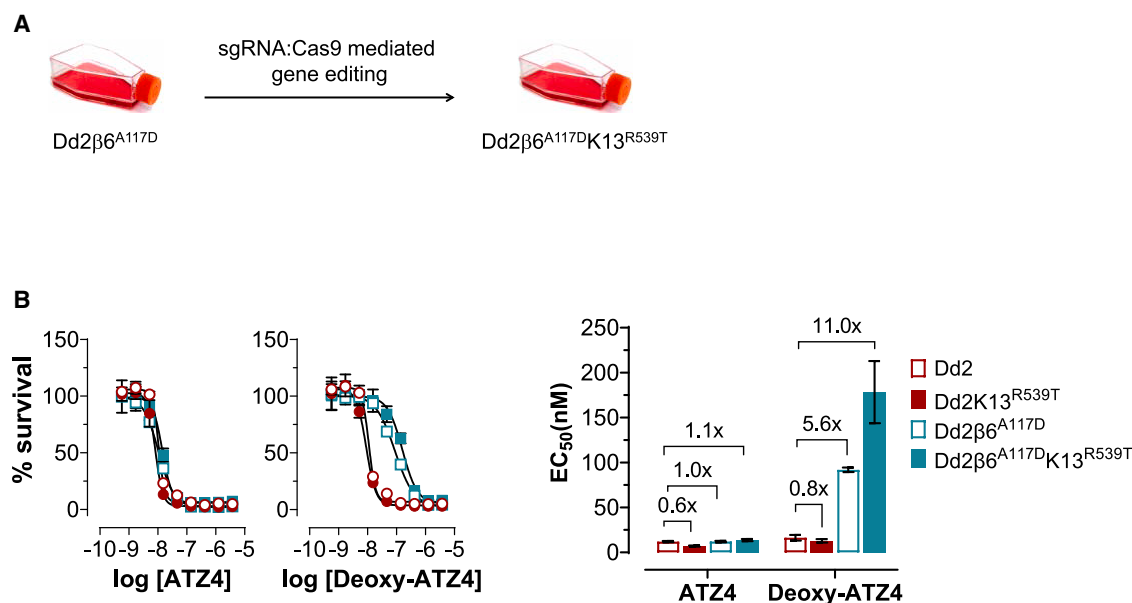
Figure 6. ATZs overcome dual resistance of *Pf* to both ART and PIs
(A) Construction of dual resistant parasite.
(B) ATZ4 but not deoxy-ATZ4 overcomes PI resistance conferred by the $\beta6^{A117D}$ mutation in the Dd2 strain bearing the ART-resistance mutation K13^{R539T}. Dose curves are representative of three independent experiments, and bar graph on the right shows the average of EC$_{50}$ ± standard error of the three experiments. Fold changes in EC$_{50}$ values are indicated above the individual bars.

SIGNIFICANCE

The complexity of ART resistance mechanisms highlights the ability of *Plasmodium* parasites to develop drug resistance. ART combination therapy has been in the clinic for decades, yet the development of ART resistance is accelerating as resistance arises to partner drugs. Even the use of triple combination therapy may not suffice to counter the emergence of resistance. Because PIs synergize with ART against *Plasmodium,* there is hope that a combination of ART and a PI could suppress the development of resistance. However, strains resistant to both a PI and ART have been developed in the laboratory without apparent loss of fitness. By stably combining a PI with an ART in a single molecule, an ATZ, the PI function proceeds in two ways—from the action of the PI moiety without activation of the ART moiety and from the action of oligopeptides bearing the PI moiety after activation of the ART moiety covalently attaches the ATZ to proteins whose damage destines them for degradation in the proteasome. These new oligopeptide-platformed PIs are retained inside the parasites, inhibit proteasome function, and kill the parasites, whether the parasites express WT proteasomes, mutant proteasomes resistant to the PI moiety, and/or K13 mutants resistant to the ART moiety.

STAR★METHODS

Detailed methods are provided in the online version of this paper and include the following:

- **KEY RESOURCES TABLE**

- **RESOURCE AVAILABILITY**
  - Lead contact
  - Materials availability
  - Data and code availability
- **EXPERIMENTAL MODELS AND SUBJECT DETAILS**
  - *Plasmodium falciparum* lines
  - *Plasmodium berghei* lines
  - *P. berghei* maintenance
  - Mouse models
- **METHOD DETAILS**
  - Materials
  - Generation of Dd2$\beta6^{A117D}$K13^{R539T}
  - *In vitro* cultivation
  - IC$_{50}$ determination
  - Antimalarial activity in erythrocytic stage
  - Ring survival assay
  - Parasite regrowth assay
  - Inhibition of Pf20S, Pf20S$\beta6^{A117D}$ and Pf20S$\beta5^{A49S}$ by PI01 and ATZ4
  - Intraparasitic hybrid activation and proteasome inhibition assay
  - HepG2 cell viability assay
  - Degradation of the modified β-casein by i-20S
  - Protein sample preparation for mass spectrometry analysis
  - LC-MS/MS
  - Mass data processing
  - Protein labeling by probes inside the parasites
  - *In vivo* efficacy of ATZ4 in mice infected with *P. berghei*
  - Recrudescence with *P. berghei* wild type and G2025^{R551T}

- ○ Compound synthesis and characterization
- ○ General procedure for HATU mediated amide bond formation
- ○ General procedure for Boc-deprotection
- ○ DeoxyART-AcOH 10
- ● QUANTIFICATION AND STATISTICAL ANALYSIS

AUTHOR CONTRIBUTIONS

Conceptualization: W.Z. and G.L.; supervision: G.L., L.A.K., H.D., A.P.W., L.C., and A.R.; investigation: W.Z., D.L., J.Y.L., S.B.S., C.Y., H.Z., J.C.H., R.W., S.Z., H.R., J.S., J.Q., G.S., L.C., N.V.S., A.P.W., A.R., H.D., C.F.N., L.A.K., and G.L.; methodology: W.Z., D.L., J.Y.L., S.B.S., C.Y., H.Z., R.W., N.V.S., A.P.W., A.R., J.Q., G.S., L.C., H.D., C.F.N., L.A.K., and G.L.; writing: W.Z., C.Y., H.D., C.F.N., L.A.K., and G.L. All authors read, edited, and approved the final manuscript.

DECLARATION OF INTERESTS

The authors declare the following competing financial interest(s): Cornell University's Center for Technology Licensing has filed a patent application on these artemisinin proteasome inhibitor hybrids. G. Lin, W. Zhan, H. Zhang, Daqiang Li, C. Nathan, and L. Kirkman are listed as inventors.

INCLUSION AND DIVERSITY

We support inclusive, diverse, and equitable conduct of research.

REFERENCES

1. WHO (2018). World Malaria Report 2018 (World Health Organization).

2. Wang, J., Zhang, C.J., Chia, W.N., Loh, C.C.Y., Li, Z., Lee, Y.M., He, Y., Yuan, L.X., Lim, T.K., Liu, M., et al. (2015). Haem-activated promiscuous targeting of artemisinin in Plasmodium falciparum. Nat. Commun. 6, 10111. https://doi.org/10.1038/ncomms10111.

3. O'Neill, P.M., Barton, V.E., and Ward, S.A. (2010). The molecular mechanism of action of artemisinin–the debate continues. Molecules 15, 1705–1721. https://doi.org/10.3390/molecules15031705.

4. Stocks, P.A., Bray, P.G., Barton, V.E., Al-Helal, M., Jones, M., Araujo, N.C., Gibbons, P., Ward, S.A., Hughes, R.H., Biagini, G.A., et al. (2007). Evidence for a common non-heme chelatable-iron-dependent activation mechanism for semisynthetic and synthetic endoperoxide antimalarial drugs. Angew. Chem. Int. Ed. Engl. 46, 6278–6283. https://doi.org/10.1002/anie.200604697.

5. Tilley, L., Straimer, J., Gnädig, N.F., Ralph, S.A., and Fidock, D.A. (2016). Artemisinin action and resistance in Plasmodium falciparum. Trends Parasitol. 32, 682–696. https://doi.org/10.1016/j.pt.2016.05.010.

6. Ismail, H.M., Barton, V., Phanchana, M., Charoensutthivarakul, S., Wong, M.H.L., Hemingway, J., Biagini, G.A., O'Neill, P.M., and Ward, S.A. (2016). Artemisinin activity-based probes identify multiple molecular targets within the asexual stage of the malaria parasites Plasmodium falciparum 3D7. Proc. Natl. Acad. Sci. USA 113, 2080–2085. https://doi.org/10.1073/pnas.1600459113.

7. Meshnick, S.R. (2002). Artemisinin: mechanisms of action, resistance and toxicity. Int. J. Parasitol. 32, 1655–1660. https://doi.org/10.1016/s0020-7519(02)00194-7.

8. Fügi, M.A., Wittlin, S., Dong, Y., and Vennerstrom, J.L. (2010). Probing the antimalarial mechanism of artemisinin and OZ277 (arterolane) with non-peroxidic isosteres and nitroxyl radicals. Antimicrob. Agents Chemother. 54, 1042–1046. https://doi.org/10.1128/AAC.01305-09.

9. Posner, G.H., Wang, D., Cumming, J.N., Oh, C.H., French, A.N., Bodley, A.L., and Shapiro, T.A. (1995). Further evidence supporting the importance of and the restrictions on a carbon-centered radical for high antimalarial activity of 1,2,4-trioxanes like artemisinin. J. Med. Chem. 38, 2273–2275. https://doi.org/10.1021/jm00013a001.

10. Bridgford, J.L., Xie, S.C., Cobbold, S.A., Pasaje, C.F.A., Herrmann, S., Yang, T., Gillett, D.L., Dick, L.R., Ralph, S.A., Dogovski, C., et al. (2018). Artemisinin kills malaria parasites by damaging proteins and inhibiting the proteasome. Nat. Commun. 9, 3801. https://doi.org/10.1038/s41467-018-06221-1.

11. Mukherjee, A., Bopp, S., Magistrado, P., Wong, W., Daniels, R., Demas, A., Schaffner, S., Amaratunga, C., Lim, P., Dhorda, M., et al. (2017). Artemisinin resistance without pfkelch13 mutations in Plasmodium falciparum isolates from Cambodia. Malar. J. 16, 195. https://doi.org/10.1186/s12936-017-1845-5.

12. Ashley, E.A., Dhorda, M., Fairhurst, R.M., Amaratunga, C., Lim, P., Suon, S., Sreng, S., Anderson, J.M., Mao, S., Sam, B., et al. (2014). Spread of artemisinin resistance in Plasmodium falciparum malaria. N. Engl. J. Med. 371, 411–423. https://doi.org/10.1056/NEJMoa1314981.

13. Müller, O., Sié, A., Meissner, P., Schirmer, R.H., and Kouyaté, B. (2009). Artemisinin resistance on the Thai-Cambodian border. Lancet 374, 1419. https://doi.org/10.1016/S0140-6736(09)61857-2.

14. Uwimana, A., Legrand, E., Stokes, B.H., Ndikumana, J.L.M., Warsame, M., Umulisa, N., Ngamije, D., Munyaneza, T., Mazarati, J.B., Munguti, K., et al. (2020). Emergence and clonal expansion of in vitro artemisinin-resistant Plasmodium falciparum kelch13 R561H mutant parasites in Rwanda. Nat. Med. 26, 1602–1608. https://doi.org/10.1038/s41591-020-1005-2.

15. Kayiba, N.K., Yobi, D.M., Tshibangu-Kabamba, E., Tuan, V.P., Yamaoka, Y., Devleesschauwer, B., Mvumbi, D.M., Okitolonda Wemakoy, E., De Mol, P., Mvumbi, G.L., et al. (2021). Spatial and molecular mapping of Pfkelch13 gene polymorphism in Africa in the era of emerging Plasmodium falciparum resistance to artemisinin: a systematic review. Lancet Infect. Dis. 21, e82–e92. https://doi.org/10.1016/S1473-3099(20)30493-X.

16. Fidock, D.A., and Rosenthal, P.J. (2021). Artemisinin resistance in Africa: how urgent is the threat? Med (N Y) 2, 1287–1288. https://doi.org/10.1016/j.medj.2021.11.005.

17. Watson, O.J., Gao, B., Nguyen, T.D., Tran, T.N.A., Penny, M.A., Smith, D.L., Okell, L., Aguas, R., and Boni, M.F. (2022). Pre-existing partner-drug resistance to artemisinin combination therapies facilitates the emergence and spread of artemisinin resistance: a consensus modelling study. Lancet. Microbe 3, e701–e710. https://doi.org/10.1016/S2666-5247(22)00155-0.

18. Straimer, J., Gnädig, N.F., Witkowski, B., Amaratunga, C., Duru, V., Ramadani, A.P., Dacheux, M., Khim, N., Zhang, L., Lam, S., et al. (2015). Drug resistance. K13-propeller mutations confer artemisinin resistance in Plasmodium falciparum clinical isolates. Science 347, 428–431. https://doi.org/10.1126/science.1260867.

19. Mok, S., Ashley, E.A., Ferreira, P.E., Zhu, L., Lin, Z., Yeo, T., Chotivanich, K., Imwong, M., Pukrittayakamee, S., Dhorda, M., et al. (2015). Drug resistance. Population transcriptomics of human malaria parasites reveals the mechanism of artemisinin resistance. Science 347, 431–435. https://doi.org/10.1126/science.1260403.

20. Birnbaum, J., Scharf, S., Schmidt, S., Jonscher, E., Hoeijmakers, W.A.M., Flemming, S., Toenhake, C.G., Schmitt, M., Sabitzki, R., Bergmann, B., et al. (2020). A Kelch13-defined endocytosis pathway mediates artemisinin resistance in malaria parasites. Science 367, 51–59. https://doi.org/10.1126/science.aax4735.

21. Yang, T., Yeoh, L.M., Tutor, M.V., Dixon, M.W., McMillan, P.J., Xie, S.C., Bridgford, J.L., Gillett, D.L., Duffy, M.F., Ralph, S.A., et al. (2019). Decreased K13 abundance reduces hemoglobin catabolism and proteotoxic stress, underpinning artemisinin resistance. Cell Rep. 29, 2917–2928.e5. https://doi.org/10.1016/j.celrep.2019.10.095.

22. Hott, A., Casandra, D., Sparks, K.N., Morton, L.C., Castanares, G.G., Rutter, A., and Kyle, D.E. (2015). Artemisinin-resistant Plasmodium falciparum parasites exhibit altered patterns of development in infected erythrocytes. Antimicrob. Agents Chemother. 59, 3156–3167. https://doi.org/10.1128/AAC.00197-15.

23. Nguyen, T.D., Olliaro, P., Dondorp, A.M., Baird, J.K., Lam, H.M., Farrar, J., Thwaites, G.E., White, N.J., and Boni, M.F. (2015). Optimum population-level use of artemisinin combination therapies: a modelling study. Lancet. Glob. Health 3, e758–e766. https://doi.org/10.1016/S2214-109X(15)00162-X.

24. Zhan, W., Visone, J., Ouellette, T., Harris, J.C., Wang, R., Zhang, H., Singh, P.K., Ginn, J., Sukenick, G., Wong, T.T., et al. (2019). Improvement of asparagine ethylenediamines as anti-malarial Plasmodium-selective proteasome inhibitors. J. Med. Chem. 62, 6137–6145. https://doi.org/10.1021/acs.jmedchem.9b00363.

25. Stokes, B.H., Yoo, E., Murithi, J.M., Luth, M.R., Afanasyev, P., da Fonseca, P.C.A., Winzeler, E.A., Ng, C.L., Bogyo, M., and Fidock, D.A. (2019). Covalent Plasmodium falciparum-selective proteasome inhibitors exhibit a low propensity for generating resistance in vitro and synergize with multiple antimalarial agents. PLoS Pathog. 15, e1007722. https://doi.org/10.1371/journal.ppat.1007722.

26. Yoo, E., Stokes, B.H., de Jong, H., Vanaerschot, M., Kumar, T., Lawrence, N., Njoroge, M., Garcia, A., Van der Westhuyzen, R., Momper, J.D., et al. (2018). Defining the determinants of specificity of Plasmodium proteasome inhibitors. J. Am. Chem. Soc. 140, 11424–11437. https://doi.org/10.1021/jacs.8b06656.

27. Xie, S.C., Gillett, D.L., Spillman, N.J., Tsu, C., Luth, M.R., Ottilie, S., Duffy, S., Gould, A.E., Hales, P., Seager, B.A., et al. (2018). Target validation and identification of novel boronate inhibitors of the Plasmodium falciparum proteasome. J. Med. Chem. 61, 10053–10066. https://doi.org/10.1021/acs.jmedchem.8b01161.

28. LaMonte, G.M., Almaliti, J., Bibo-Verdugo, B., Keller, L., Zou, B.Y., Yang, J., Antonova-Koch, Y., Orjuela-Sanchez, P., Boyle, C.A., Vigil, E., et al. (2017). Development of a potent inhibitor of the Plasmodium proteasome with reduced mammalian toxicity. J. Med. Chem. 60, 6721–6732. https://doi.org/10.1021/acs.jmedchem.7b00671.

29. Li, H., O'Donoghue, A.J., van der Linden, W.A., Xie, S.C., Yoo, E., Foe, I.T., Tilley, L., Craik, C.S., da Fonseca, P.C.A., and Bogyo, M. (2016). Structure- and function-based design of Plasmodium-selective proteasome inhibitors. Nature 530, 233–236. https://doi.org/10.1038/nature16936.

30. Li, H., van der Linden, W.A., Verdoes, M., Florea, B.I., McAllister, F.E., Govindaswamy, K., Elias, J.E., Bhanot, P., Overkleeft, H.S., and Bogyo, M. (2014). Assessing subunit dependency of the Plasmodium proteasome using small molecule inhibitors and active site probes. ACS Chem. Biol. 9, 1869–1876. https://doi.org/10.1021/cb5001263.

31. Li, H., Tsu, C., Blackburn, C., Li, G., Hales, P., Dick, L., and Bogyo, M. (2014). Identification of potent and selective non-covalent inhibitors of the Plasmodium falciparum proteasome. J. Am. Chem. Soc. 136, 13562–13565. https://doi.org/10.1021/ja507692y.

32. Kirkman, L.A., Zhan, W., Visone, J., Dziedziech, A., Singh, P.K., Fan, H., Tong, X., Bruzual, I., Hara, R., Kawasaki, M., et al. (2018). Antimalarial proteasome inhibitor reveals collateral sensitivity from intersubunit interactions and fitness cost of resistance. Proc. Natl. Acad. Sci. USA 115, E6863–E6870. https://doi.org/10.1073/pnas.1806109115.

33. Santos, R.d.L.A., Bai, L., Singh, P.K., Murakami, N., Fan, H., Zhan, W., Zhu, Y., Jiang, X., Zhang, K., Assker, J.P., et al. (2017). Structure of human immunoproteasome with a reversible and noncompetitive inhibitor that selectively inhibits activated lymphocytes. Nat. Commun. 8, 1692. https://doi.org/10.1038/s41467-017-01760-5.

34. Zhan, W., Zhang, H., Ginn, J., Leung, A., Liu, Y.J., Michino, M., Toita, A., Okamoto, R., Wong, T.T., Imaeda, T., et al. (2021). Development of a highly selective Plasmodium falciparum proteasome inhibitor with anti-malaria activity in humanized mice. Angew. Chem. Int. Ed. Engl. 60, 9279–9283. https://doi.org/10.1002/anie.202015845.

35. Simwela, N.V., Stokes, B.H., Aghabi, D., Bogyo, M., Fidock, D.A., and Waters, A.P. (2020). Plasmodium berghei K13 mutations mediate in vivo artemisinin resistance that is reversed by proteasome inhibition. mBio 11, e02312-20. https://doi.org/10.1128/mBio.02312-20.

36. Davis, S.Z., Singh, P.P., Vendrely, K.M., Shoue, D.A., Checkley, L.A., McDew-White, M., Button-Simons, K.A., Cassady, Z., Sievert, M.A.C., Foster, G.J., et al. (2020). The extended recovery ring-stage survival assay provides a superior association with patient clearance half-life and increases throughput. Malar. J. 19, 54. https://doi.org/10.1186/s12936-020-3139-6.

37. Verdoes, M., Florea, B.I., Menendez-Benito, V., Maynard, C.J., Witte, M.D., van der Linden, W.A., van den Nieuwendijk, A.M.C.H., Hofmann, T., Berkers, C.R., van Leeuwen, F.W.B., et al. (2006). A fluorescent broad-spectrum proteasome inhibitor for labeling proteasomes in vitro and in vivo. Chem. Biol. 13, 1217–1226. https://doi.org/10.1016/j.chembiol.2006.09.013.

38. Rosenthal, M.R., and Ng, C.L. (2021). A proteasome mutation sensitizes P. falciparum Cam3.II K13(C580Y) parasites to DHA and OZ439. ACS Infect. Dis. 7, 1923–1931. https://doi.org/10.1021/acsinfecdis.0c00900.

39. Xie, S.C., Metcalfe, R.D., Mizutani, H., Puhalovich, T., Hanssen, E., Morton, C.J., Du, Y., Dogovski, C., Huang, S.C., Ciavarri, J., et al. (2021). Design of proteasome inhibitors with oral efficacy in vivo against Plasmodium falciparum and selectivity over the human proteasome. Proc. Natl. Acad. Sci. USA 118. e2107213118. https://doi.org/10.1073/pnas.2107213118.

40. Garg, S., Kreutzfeld, O., Chelebieva, S., Tumwebaze, P.K., Byaruhanga, O., Okitwi, M., Orena, S., Katairo, T., Nsobya, S.L., Conrad, M.D., et al. (2022). Susceptibilities of Ugandan Plasmodium falciparum isolates to proteasome inhibitors. Antimicrob. Agents Chemother. 66, e0081722. https://doi.org/10.1128/aac.00817-22.

41. Leroy, D. (2017). How to tackle antimalarial resistance? EMBO Mol. Med. 9, 133–134. https://doi.org/10.15252/emmm.201607295.

42. Burrows, J.N., Duparc, S., Gutteridge, W.E., Hooft van Huijsduijnen, R., Kaszubska, W., Macintyre, F., Mazzuri, S., Möhrle, J.J., and Wells, T.N.C. (2017). New developments in anti-malarial target candidate and product profiles. Malar. J. 16, 26. https://doi.org/10.1186/s12936-016-1675-x.

43. Nathan, C. (2017). Kunkel lecture: fundamental immunodeficiency and its correction. J. Exp. Med. 214, 2175–2191. https://doi.org/10.1084/jem.20170637.

44. Lin, G., Li, D., de Carvalho, L.P.S., Deng, H., Tao, H., Vogt, G., Wu, K., Schneider, J., Chidawanyika, T., Warren, J.D., et al. (2009). Inhibitors selective for mycobacterial versus human proteasomes. Nature 461, 621–626. https://doi.org/10.1038/nature08357.

45. White, N.J. (2010). Artemisinin resistance–the clock is ticking. Lancet 376, 2051–2052. https://doi.org/10.1016/S0140-6736(10)61963-0.

46. Breman, J.G. (2012). Resistance to artemisinin-based combination therapy. Lancet Infect. Dis. *12*, 820–822. https://doi.org/10.1016/S1473-3099(12)70226-8.

47. Phyo, A.P., Nkhoma, S., Stepniewska, K., Ashley, E.A., Nair, S., McGready, R., ler Moo, C., Al-Saai, S., Dondorp, A.M., Lwin, K.M., et al. (2012). Emergence of artemisinin-resistant malaria on the western border of Thailand: a longitudinal study. Lancet *379*, 1960–1966. https://doi.org/10.1016/S0140-6736(12)60484-X.

48. Uhlemann, A.C., and Fidock, D.A. (2012). Loss of malarial susceptibility to artemisinin in Thailand. Lancet *379*, 1928–1930. https://doi.org/10.1016/S0140-6736(12)60488-7.

49. Tulloch, J., David, B., Newman, R.D., and Meek, S. (2013). Artemisinin-resistant malaria in the Asia-Pacific region. Lancet *381*, e16–e17. https://doi.org/10.1016/S0140-6736(12)61820-0.

50. The, L. (2014). Time to contain artemisinin resistance. Lancet *383*, 1438. https://doi.org/10.1016/S0140-6736(14)60700-5.

51. van der Pluijm, R.W., Imwong, M., Chau, N.H., Hoa, N.T., Thuy-Nhien, N.T., Thanh, N.V., Jittamala, P., Hanboonkunupakarn, B., Chutasmit, K.,

Saelow, C., et al. (2019). Determinants of dihydroartemisinin-piperaquine treatment failure in Plasmodium falciparum malaria in Cambodia, Thailand, and Vietnam: a prospective clinical, pharmacological, and genetic study. Lancet Infect. Dis. *19*, 952–961. https://doi.org/10.1016/S1473-3099(19)30391-3.

52. van der Pluijm, R.W., Tripura, R., Hoglund, R.M., Pyae Phyo, A., Lek, D., Ul Islam, A., Anvikar, A.R., Satpathi, P., Satpathi, S., Behera, P.K., et al. (2020). Triple artemisinin-based combination therapies versus artemisinin-based combination therapies for uncomplicated Plasmodium falciparum malaria: a multicentre, open-label, randomised clinical trial. Lancet *395*, 1345–1360. https://doi.org/10.1016/S0140-6736(20)30552-3.

53. Franke-Fayard, B., Janse, C.J., Cunha-Rodrigues, M., Ramesar, J., Büscher, P., Que, I., Löwik, C., Voshol, P.J., den Boer, M.A.M., van Duinen, S.G., et al. (2005). Murine malaria parasite sequestration: CD36 is the major receptor, but cerebral pathology is unlinked to sequestration. Proc. Natl. Acad. Sci. USA *102*, 11468–11473. https://doi.org/10.1073/pnas.0503386102.

STAR★METHODS

KEY RESOURCES TABLE

REAGENT or RESOURCE	SOURCE	IDENTIFIER
Chemicals, peptides, and recombinant proteins		
PI01	This paper	N/A
ART1	This paper	N/A
ATZ2	This paper	N/A
ATZ4	This paper	N/A
Deoxy-ATZ4	This paper	N/A
ATZ-P1	This paper	N/A
Deoxy-ATZ-P1	This paper	N/A
Artemisinin	Sigma-Aldrich	Catalog # 361593
Hemin	Sigma-Aldrich	Catalog # 51280
Sodium ascorbate	Sigma-Aldrich	Catalog # PHR1279
Activity-based probe MV151	Verdoes et al.[37]	N/A
β2-specific inhibitor WLW-VS	Li et al.[29]	N/A
Suc-LLVY-AMC	Boston Biochem	Catalog # S-280
Ac-ANW-AMC	Boston Biochem	Catalog # S-320
Trypsin	Promega	Catalog #V528A
Chymotrypsin	Promega	Catalog #V106A
Human constitutive proteasome	Boston Biochem	Catalog # E−360
Human 20S immunoproteasome	Boston Biochem	Catalog # E−370
Recombinant human PA28 activator alpha subunit	Boston Biochem	Catalog # E−381
P. falciparum 20S proteasome	Kirkman et al.[32]	N/A
β-Casein	Sigma-Aldrich	Catalog #C6905
Bovine serum albumin	Sigma-Aldrich	Catalog # 3117057001
12% Novex™ Bis-Tris Protein Gel	ThermoFisher Scientific	Catalog # NP0341BOX
MOPS SDS running buffer	ThermoFisher Scientific	Catalog # NP0001
Mini cOmplete EDTA-free Protease Inhibitor Cocktail	Sigma-Aldrich	Catalog # 11836170001
Critical commercial assays		
Pierce BCA Protein Assay Kit	ThermoFisher Scientific	Catalog # 23225
CellTiter-Glo® Assay Kit	Promega	Catalog #G7573
Experimental models: Cell lines		
HepG2 cell	ATCC	HB-8065™
Experimental models: Organisms/strains		
Plasmodium falciparum Dd2	BEI Resources	MRA-150
Plasmodium falciparum Cam3.1^{R539T}	BEI Resources	MRA-1255
Plasmodium falciparum strain Cam3.1^{Rev}	BEI Resources	MRA-1252
Plasmodium falciparum Dd2 β6^{A117D}	Kirkman et al.[32]	N/A
Plasmodium falciparum Dd2 β^{A49S}	Zhan et al.[24]	N/A
Plasmodium berghei ANKA Lux	Franke-Fayard et al.[53]	N/A
Plasmodium berghei G2025^{R551T}	Simwela et al., 2021	N/A
Plasmodium berghei G1989^{M488I}	Simwela et al., 2021	N/A
Plasmodium falciparum Dd2 β6^{A117D}K13^{R539T}	This paper	N/A
Swiss Webster (CFW) Mouse	Charles River	CFW(024)
Oligonucleotides		
Single guide 1 sequence: ATGATCGTTTAAGAGATGTA	This paper	N/A
Single guide 2 sequence: ATACCTAGAAGAAATAATTG	This paper	N/A

Continued

REAGENT or RESOURCE	SOURCE	IDENTIFIER
Single guide 3 sequence: *TGATCATCGTATGAAAGCAT*	This paper	N/A
Repair template (Single guides are underlined and shield mutations are in bold) ATAGGTGGATTTGATGGTGTAGA ATATTTAAATTCGATGGAATTATTAGATATTAGTCAACAA TGCTGGCGTATGTGTACACCTATGTCTACCAAAAAAGC TTATTTTGGAAGTGCTGTATTGAATAATTTCTTATACGTT TTTGGTGGTAATAACTATGATTATAAGGCTTTATTTGAA ACTGAGGTGT<u>ATGATCGTTTA**CGT**GA**C**G**TC**</u>TGGTATGT TTCAAGTAATTTAAAT<u>ATACCTAGAAGAAA**CAAC**TGC</u>GG TGTTACGTCAAATGGTACAATTTATTGTATTGGGGGATA TGATGGCTCTTCTATTATACCGAATGTAGAAGCATA<u>TGA</u> <u>TCAT**AGA**ATGAA**G**GC**T**T</u>GGGTAGAGGTGGCACCTTTGA ATACCCCTAGATCATCAGCTATGTGTGTTGCTTTTGATA ATAAAATTTATGTCATTGGTGGAACTAATGGTGAGAGA TTAAATTCTATTGAAGTATATGAAGAAAAAATGAATAA ATGGGAACAATTTCCATATGCCTTATTAGAAGCT AGAAGTTCA	This paper	N/A
Software and algorithms		
ImageJ	Schneider et al.[7]	https://imagej.nih.gov/ij/
Chemdraw Pro	PerkinElmer	https://perkinelmerinformatics.com/products/research/chemdraw
GraphPad Prism 9	GraphPad Software Inc.	https://www.graphpad.com/
Microsoft Office Suite	Microsoft, Inc.	N/A
Other		
Slide-A-Lyzer MINI Dialysis Devices	ThermoFisher Scientific	Catalog # 88401

RESOURCE AVAILABILITY

Lead contact
Further information and requests for resources and reagents should be directed to and will be fulfilled by the lead contact, Gang Lin, gal2005@med.cornell.edu.

Materials availability
All unique/stable reagents generated in this study are available from the lead contact with a completed Materials Transfer Agreement.

Gang Lin, PhD, gal2005@med.cornell.edu; small aliquots of all chemicals including ATZ-P1 and deoxy-ATZ-P1 are available for request.

Laura Kirkman, MD, lak9015@med.cornell.edu; Pf Dd2 β6^{A117D}, Pf Dd2 ^{β5A49S} and Dd2 β6^{A117D}K13^{R539T} are available for request.

Data and code availability
- All data reported in this paper will be shared by the lead contact upon request. Uncropped western blot images are reported in supplemental information.
- This paper does not report original code.
- Any additional information required to reanalyze the data reported in this paper is available from the lead contact upon request.

EXPERIMENTAL MODELS AND SUBJECT DETAILS

Plasmodium falciparum lines
3D7, Dd2, Cam 3.1^{R539T}, and Cam3.1^{Rev} were obtained from BEI Resources.

Plasmodium berghei lines
G2025^{R551T} and G1989^{M488I} were obtained from Dr. Andrew P Waters.

P. berghei maintenance

Female Swiss Webster mice 6–8 weeks old were infected by i.p. inoculation of 3×10^6 erythrocytes infected with *P. berghei* ANKA wt or lines G2025[R551T] and G1989[M488I] from frozen vials. When parasitemia reached >20%, mice were sacrificed and blood was used either for infection of experimental mice or stored at $-80°C$.

Mouse models

Swiss Weber female mice 6 to 8 weeks were obtained from Charles River and the studies were carried out in accordance with the guidance from New York University IACUC board of regulations, respecting all ethical regulations.

P. berghei infection model

Female Swiss Webster mice 6–8 weeks old were infected by i.p. inoculation of 1×10^3 erythrocytes infected with *P. berghei* ANKA expressing luciferase.[53] One day after administration of the last treatment dose, mice were anesthetized by inhalation of isoflurane, injected i.p. with 150 mg/kg of D-Luciferin in PBS and imaged 5 to 10 min later with an IVIS 100 (Xenogen, Alameda, CA).

Modified Peters' 4-day suppression test for recrudescence in mice: Female Swiss Webster mice 6–8 weeks old were infected by i.p. inoculation of 1.5×10^5 erythrocytes infected with *P. berghei* ANKA wt or 1×10^6 erythrocytes infected with *P. berghei* lines G2025[R551T] from recently sacrificed donor mice (not from frozen vials). Parasitemias were quantified by microscopy of Giemsa-stained blood smears from tail vein.

METHOD DETAILS

Materials

The human constitutive proteasome (c-20S, Catalog No.: E−360), human 20S immunoproteasome (i-20S, Catalog No.: E−370), and recombinant human PA28 activator alpha subunit (Catalog N0.: E−381) were purchased from Boston Biochem. The *P. falciparum* 20S proteasome (*Pf*20S) was purified as reported.[32] β-Casein (Catalog No.: C6905), bovine serum albumin (BSA, Catalog No.: 3117057001), hemin (Catalog No.:51280), sodium ascorbate (Catalog No.: PHR1279), artemisinin (ART, Catalog No.: 361593) and artesunate (ASU, Catalog No.: A3731) were purchased from Sigma-Aldrich. Trypsin (V528A) or chymotrypsin (V106A) were purchased from Promega. Proteasome β5 substrate suc-LLVY-AMC and β5i substrate Ac-ANW-AMC were purchased from Boston Biochem. Activity-based probe MV151 was synthesized as reported.[37] β2-specific inhibitor WLW-VS was prepared following the reported method.[29]

The following parasite strains were obtained through BEI Resources, National Institute of Allergy and Infectious Disease, National Institutes of Health: *P. falciparum*; strain IPC 5202, MRA-1240 contributed by Didier Ménard and strain Cam3.I[rev], MRA-1252, contributed by David A. Fidock. IPC 5202 is also referred to as Cam 3.1[R539T] and has shown resistance to artemisinin and harbors a K13 propeller mutation of R539T. Cam3.I[rev] is a K13-propeller revertant mutant of the original Cam 3.1 strain.

Generation of Dd2ß6[A117D]K13[R539T]

Dd2ß6[A117D]K13[R539T] parasite line was generated by CRISPR-Cas9 mediated single nucleotide replacement (R539T) in k13gene. Dd2ß6[A117D] parasites were co-transfected with pL6-K13[R539T] plasmid (a donor DNA template, carrying K13R539T mutation and shield mutation. The shield mutation is silent but abolishes recognition by Cas9, thereby protecting the modified locus from repeated cleavage) and pUF1-Cas9-sgRNA plasmid (containing Cas9 expression cassette and single guides). To have a robust Cas9 editing, three different single guides were selected (sg1, 2 and 3) as the Cas9-target site. Selection was carried out using Blasticidin (2 μg/mL) and DSM1(1.6μM/10mL) until viable parasites were recovered by blood smear. Successful editing of the genomic K13 locus was verified by PCR and sanger sequencing.

In vitro cultivation

P. falciparum laboratory lines were grown under standard conditions in RPMI 1640 medium with 0.5% Albumax II (Invitrogen), 5% hematocrit, 0.25% sodium bicarbonate and 0.1 mg/mL gentamicin. Parasites were placed in an incubator under 90% nitrogen, 5% carbon dioxide and 5% oxygen at 37°C. Two Dd2-derived resistant strains (Dd2ß5[A49S] and Dd2ß6[A117D]) were developed in-house and identified as described.[24,32]

IC50 determination

IC$_{50}$ values of all compounds against Pf20S β5, human c-20S β5c and i-20S β5i were determined in a 96-well format as described.[24,32,33] Briefly, 1 μL of compound in a 3-fold series dilution in DMSO at final concentrations from 100 μM to 0.0017 μM was mixed with 99 μL of reaction buffer containing the corresponding proteasome, substrate and activator in a black 96-well plate with a solid bottom. Buffer 50 mM Tris, 5 mM MgCl$_2$, 1 mM DTT, pH 7.4 was for Pf20S β5 and buffer 20 mM HEPES, 0.5 mM EDTA and 0.1 mg/mL BSA, pH7.5 for human β5c and β5i. The fluorogenic substrate suc-LLVY-AMC was used for Pf20S and c-20S at final concentration 25 μM, and Ac-ANW-AMC was used as substrate of i-20S at final concentration 15 μM. Activator PA28α at final concentration of 12 nM was used for Pf20S assay in the presence of 0.5 μM of WLW-VS, whereas 0.02% SDS was used in the assays for c-20S and i-20S. Final concentrations of Pf20S, c-20S and i-20S were 1 nM, 0.2 nM and 0.4 nM, respectively. The fluorescence of the

hydrolyzed AMC at $\lambda ex = 360nm$ and $\lambda ex = 460$ nm in each well was followed for 1–2 h. Linear ranges of the time course were used to calculate the velocities in each well, which were fit to a dose-dependent inhibition equation to estimate the IC_{50} values in PRISM (GraphPad).

Antimalarial activity in erythrocytic stage

Parasite growth inhibition assays were performed as reported.[32] Drug assays were performed on parasites cultured in sterile 96-well plates at a total 200 μL volume per well and a 0.5% initial parasitemia and 2% hematocrit. Plates were placed in an airtight chamber flushed with 5% oxygen, 5% carbon dioxide and 90% nitrogen for 72 h. Plates were then placed in the $-80°C$ freezer to promote cell lysis upon thawing. When thawing was complete, 100 μL of SYBR Green diluted in lysis buffer (0.2 μL SYBR Green per mL lysis buffer) was added to each well and the plates were shaken in the dark at room temperature for 1 h. Fluorescence was then recorded in a SpectraMax Gemini plate reader using $\lambda ex = 490$ nm/$\lambda em = 530$ nm. Data analysis was performed with Graphpad Prism software. Counts were normalized and plotted by non-linear regression to yield EC_{50} values.

Ring survival assay

Ring survival assays (RSA) were performed as described.[18] Parasite cultures, IPC5202 (Cam3.I^{R539T}), an artemisinin resistant parasite line from Cambodia, and the genetically engineered artemisinin sensitive revertant Cam3.I^{rev}, were synchronized several times with 5% sorbitol and then a Percoll-sorbitol gradient was used to obtain tightly synchronized late-stage parasites. Isolated late-stage parasites were then allowed to reinvade fresh red blood cells for 3 h ring stage parasites were confirmed by microscopy before the cultures were again subjected to 5% sorbitol to obtain 0-3 h rings. The isolated ring stage cultures were then plated into a 96 well plate at 0.5% parasitemia at the corresponding drug concentrations: DHA 700 nM, PI01 800 nM, ART1 800 nM, ATZ4 700 nM. Plates were incubated at $37°C$ in standard gas conditions for 6 h before the plates were spun and washed to remove medium with compound and replenished with fresh medium. Plates were then incubated for an additional 66 h and parasite growth was then assessed using flow cytometry and nucleic acid stains HO (Hoechst 33342) and TO (thiazole orange).

Parasite regrowth assay

Parasite culutres were synchronized as described for the RSA and treated with the same drug concentrations for 6 h in a 96 well plate. After 6 h of drug/compound exposure and washing, the 200 μL culture was then transferred to a 3 mL culture which was monitored for seven days. Parasitemia was checked by microscopy on day 7.

Inhibition of Pf20S, Pf20Sβ6^{A117D} and Pf20Sβ5^{A49S} by PI01 and ATZ4

Frozen *Pf* pellets of Dd2 wild-type and two Dd2-derived resistant (Dd2β5^{A49S} and Dd2β6^{A117D}) were thawed on ice and resuspended in 2x pellet volume of lysis buffer (pH 7.4) containing 50 mM Tris-HCl, 5 mM $MgCl_2$, and 1mM DTT, respectively. The mixtures were kept on ice for 1 h and vigorously vortexed every 10 min, then centrifuged at 15,000 rpm for 15 min at $4°C$. The supernatants were collected and stored at $-80°C$ for later use. Their concentrations were determined by BCA protein assay. 5–10 μg of total lysate proteins were incubated with PI01 or ATZ4 at the indicated concentrations for 1 h at $37°C$ prior to addition of MV151 at a final concentration of 2 μM and incubated for a further 1 h at $37°C$ (avoid the light after adding MV151 and last until the end of this experiment). The samples were then heated with 4X SDS loading buffer at $95°C$ for 10 min and run on 12% Novex Bis-Tris Protein Gels with MOPS SDS running buffer. The gels were rinsed with double distilled H_2O and then scanned at the Cy3/TAMRA settings (λ_{ex} 532 nm, λ_{em} 560 nm) on a Typhoon Scanner.

Intraparasitic hybrid activation and proteasome inhibition assay

Pf Dd2, Dd2β6^{A117D} and Dd2β5^{A49S} parasites were grown synchronized to a high parasitemia (5–8%). At the early trophozoite stage, 5 mL of parasite-infected red blood cells were exposed to DMSO, PI01 (800 nM), ART1 (800 nM), ATZ4 (700 nM), and a mixture of ART1 and PI01 in a 1:1 ratio both at 800 nM for 6 h. After centrifugation at 3600 rpm for 3 min, the supernatant was removed, and red cells were washed with complete media once and resuspended in 14 mL of fresh complete media. The cultures were then placed back in the incubator and shaken for 10 min. The wash procedure was repeated 4 times. After the last wash, the red blood cell pellets were placed on ice and washed with PBS 1 mL once and then lysed with 10% saponin to obtain parasite pellets. Parasite pellets were kept on ice and washed with cold PBS until supernatant was clear (approximately 3 times). Pellets were stored at $-80°C$ until analysis. The frozen *Pf* pellets were thawed on ice and resuspended in 2 x pellet volume of lysis buffer containing 20 mM Tris-HCl, 5 mM $MgCl_2$ and 1 mM DTT, pH 7.4. The mixtures were kept on ice for 1 h and vigorously vortexed every 5 min, then centrifuged at 15000 rpm for 20 min at $4°C$. The supernatants were collected, and their concentrations were determined by BCA protein assay. Equal amounts of lysates were incubated with MV151 at a final concentration of 2 μM for 1 h at $37°C$ in a 1.5 mL Eppendorf tube wrapped in aluminum foil. The samples were then heated with 4X SDS loading buffer at $95°C$ for 10 min and run on a 12% Novex Bis-Tris Protein Gel with MOPS SDS running buffer. The gel was rinsed with double distilled H_2O and scanned at the TAMRA channel on a Typhoon Scanner (GE Healthcare). In an alternative procedure, wash steps of parasite-infected red blood cells in the above-stated procedure were omitted to examine the permeability of PI01 and ATZ4. However, parasite pellets were thoroughly washed to remove red blood cell constituents to avoid interferences in the MV151 labeling assays.

HepG2 cell viability assay

HepG2 cells were plated in 96-well plate (5,000 cells per well) format and treated with various concentrations of test compounds or DMSO for 72 h. Cell viability was measured using CellTiter-Glo Assay (Promega) as per the manufacturer's instructions.

Degradation of the modified β-casein by i-20S

β-casein dissolved in PBS (10 μM) was incubated with 100 μM of PI01, ART1 or ATZ2 in the presence of sodium ascorbate (200 μM) and hemin (100 μM) at r.t. for 4 h. The samples were transferred to Slide-A-Lyzer MINI Dialysis Devices (10K MWCO, Thermo Scientific 88401) and placed into tubes containing the dialysis buffer (20 mM HEPES and 0.5 mM EDTA, pH7.5) and dialyzed overnight at 4°C with fresh dialysis buffer changing every 4 h. After dialysis, the samples were collected and further incubated with i-20S (50 nM), PA28α (0.5 μM), and bovine serum albumin (10 μM) at 37°C. Aliquots from the reaction mixtures were removed at designated time intervals, mixed with SDS sample loading buffer, and were run on an SDS-PAGE (4–20%, Tris-Glycine) and stained with Coomassie blue. For the control experiment in Figure 2B, samples were prepared with the same method above, except that dialysis step was skipped.

Protein sample preparation for mass spectrometry analysis

β-casein was treated as aforementioned. After removing the inhibitors, hemin and ascorbate by dialysis, the treated β-casein samples were run on SDS-page and stained with Coomassie blue G-250. The gel bands of β-casein were cut into pieces. Samples were reduced with 5 mM dithiothreitol in 50 mM ammonium bicarbonate buffer for 50 min at 55°C and then dried by acetonitrile. Next, the samples were alkylated with 12.5 mM iodoacetamide in 50 mM ammonium bicarbonate buffer for 45 min in the dark at room temperature and dried by acetonitrile. The samples were then digested by trypsin or chymotrypsin at 37°C overnight. The digestion was stopped with 10% trifluoracetic acid, after which the digested peptides were extracted twice with 1% formic acid in 50% acetonitrile aqueous solution, and then evaporated to dryness on a Speedvac and resuspended in 20 μL of formic acid/H_2O (v/v = 0.1%/99.9%) with sonication.

LC-MS/MS

For LC-MS/MS analysis, the fragment peptides were separated by a 120-min gradient elution method at a flow rate of 0.3 μL/min with a Thermo-Dionex Ultimate 3000 HPLC system that is directly interfaced with a Thermo Orbitrap Fusion Lumos mass spectrometer. The analytical column was a homemade fused silica capillary (75 μm inner-diameter, 150 mm length; Upchurch, Oak Harbor, WA, USA) packed with C-18 resin (pore size 300 Å, particle size 5 μm; Varian, Lexington, MA, USA). Mobile phase A was 0.1% formic acid in water, and mobile phase B is 100% acetonitrile and 0.1% formic acid. The Thermo Orbitrap Fusion Lumos mass spectrometer was operated in the data-dependent acquisition mode using Xcalibur 4.0.27.10 software. A single full-scan mass spectrum was done in the Orbitrap (300–1500 m/z, 120,000 resolution). The spray voltage was 1850 V and the Automatic Gain Control (AGC) target was 200,000. This was followed by 3-s data-dependent MS/MS scans in an ion routing multipole at 30% normalized collision energy (HCD). The charge state screening of ions was set at 1–8. The exclusion duration was set at 8 s. Mass window for precursor ion selection was set at 2 m/z. The MS/MS resolution was 15,000. The MS/MS maximum injection time was 150 ms and the AGC target was 50,000.

Mass data processing

Data were searched against the bovine casein database from the Uniprot by using Proteome Discoverer 1.4 software (Thermo Scientific) and peptide sequences were determined by matching protein database with the acquired fragmentation pattern by SEQUEST HT algorithm. The following search parameters were used: the precursor mass tolerance was set to 10 ppm and fragment mass tolerance was 0.02 Da; No-Enzyme (Unspecific); Modification (MOD) A_1 (811.39624 Da, Table S1, any amino acids), MOD A_2 (751.37511 Da, Table S1, any amino acids), MOD B_1 (325.18837 Da, Table S1, any amino acids), MOD B_2 (265.16725 Da, Table S1, any amino acids), carbamidomethyl of cysteines (+57.02146 Da), oxidation of methionines (+15.99492 Da) as the variable modifications. Only peptides with the strict target false discovery rate (FDR) below 1% were considered as high-confidence hits.

Protein labeling by probes inside the parasites

Fifty mL of *Pf* Dd2 parasites in red blood cells were treated with ATZ-P1 (700 nM), deoxy-ATZ-P1 (700 nM) and ART (700 nM) for 6 h. After washing off the excessive compounds, red blood cells were placed on ice and washed with PBS 1 mL once and then lysed with 10% saponin to obtain parasite pellets. Parasite pellets were kept on ice and washed with cold PBS until supernatant was clear (approximately 3 times). Pellets were stored at −80°C until analysis. Frozen *Pf* pellets were thawed on ice and resuspended in 2x pellet volume of lysis buffer (pH 7.4) containing 50 mM Tris-HCl, 5 mM MgCl2, and a protease inhibitor mixture (Mini cOmplete EDTA-free Protease Inhibitor Cocktail, Sigma). The mixtures were kept on ice for 1 h and vigorously vortexed every 10 min, followed by trituration with a sonicator probe on ice (∼4°C), then centrifuged at 15,000 rpm for 15 min at 4°C. The supernatants were collected and stored at −80°C for later use. Their concentrations were determined by BCA protein assay. For each click reaction, the lysate (1.5 mg/mL, 44 μL) was successively mixed with 0.5 μL Cy3 alkyne (2 mM stock in DMSO), 3.3 μL Tris[(1-benzyl-1H-1,2,3-triazol-4-yl) methyl]amine (TBTA, 1.7 mM stock in DMSO:t-butanol 1:4), 1.0 μL CuSO4 (50 mM stock in ddH2O), and 1.0 μL Tris(2-carboxyethyl) phosphine (TCEP, 50 mM stock in ddH2O). Each reaction was then gently vortexed and allowed to react at room temperature for 1 h in the dark, with regular vortexing every 10 min. Novex 16% Tricine Mini Protein Gels (Invitrogen) were used for protein separation with

Tricine SDS running buffer (Invitrogen), and spectra multicolor low range protein ladder as protein marker. After boiling with loading buffer, 20 μL of each sample were used for electrophoresis. After rinsing with double distilled H2O, the gel was scanned at TAMRA channel on a Typhoon Scanner (GE Healthcare) with a Cy3 filter. Equal protein loading was confirmed by post scan staining with Coomassie blue (Pierce, UK).

In vivo efficacy of ATZ4 in mice infected with *P. berghei*

Female 6–8 weeks old Swiss-Webster mice were infected on day 0 via *i.p.* injection with 10^3 ($\sim 5 \times 10^5$% infection) *P. berghei*-Luccon[53] infected erythrocytes. Treatments started from day 3 to day 6 for 4 days. Chloroquine (20 mg/kg) in 0.5% hydroxymethyl cellulose, 0.4% Tween-80 and ATZ4 (10, 25, 50 mg/kg) in 5% DMSO, 5% Tween-80 in sterile water were administered via *i.p.* once daily. On day 7, anesthetized mice were i.p. injected 150 mg/kg of D-luciferin potassium-salt (Goldbio, LUCK-100) dissolved in PBS. Mice were imaged 5 to 10 min after injection of luciferin with an IVIS 100 (Xenogen, Alameda, CA) and the data acquisition and analysis were performed with the software LivingImage (Xenogen).

Recrudescence with *P. berghei* wild type and G2025^{R551T}

Female 6–8 weeks old Swiss-Webster mice were infected on day 0 via *i.p.* injection with 1.6×10^5 ($\sim 5 \times 10^5$% infection) *P. berghei*-Luccon[53] infected erythrocytes, or 1×10^6 *P berghei* G2025^{R551T}. Treatments started 3 h post inoculation on day 0 and continued to day 2 for 3 days. ART (50 mg/kg) in 0.5% hydroxymethyl cellulose, 0.4% Tween-80, ATZ4 (100 or 125 mg/kg) in 5% DMSO, 5% Tween-80 in sterile water, and deoxy-ATZ4 (100 or 125 mg/kg) in 5% DMSO, 5% Tween-80 sterile water were administered via *i.p.* once daily. Parasitemia was monitored by Giemsa-stained smears on day 6, 8, 10, 16 and 21.

### Compound synthesis and characterization
Chemicals and spectroscopy

Unless otherwise stated, all commercially available materials were purchased from Aldrich, P3 BioSystems, Combi-Blocks or other vendors and were used as received. All reactions in aprotic solvents were performed under argon in oven-dried glassware. Reaction progress was monitored on a Waters Acquity Ultra Performance Liquid Chromatography (UPLC/MS). All HPLC purifications were performed on a Waters Autopure (mass directed purification system) equipped with a Prep C18 5μm OBD (19 × 150 mm) column. ^{1}H- and ^{13}C- NMR spectra were acquired on a Bruker DRX-500 spectrometer. Chemical shift δ is expressed in parts per million, with the solvent resonance as an internal standard (CDCl$_3$, ^{1}H: 7.26; ^{13}C: 77.16 ppm; DMSO-*d6*, ^{1}H: 2.50 ppm; ^{13}C: 39.52 ppm). NMR data are reported as follows: chemical shift, multiplicity (br = broad, d = doublet, q = quartet, m = multiplet, s = singlet, t = triplet), coupling constant, and integration. High Resolution Mass Spectra (HRMS) of final products were collected on a PE SCIEX API 100.

General procedure for HATU mediated amide bond formation

The solution of carboxylic acid (1.1 equiv) and *O*-(7-azabenzotriazol-1-yl)-*N,N,N,N'*-tetramethyluronium hexafluorophosphate (HATU, 1.5 equiv) in anhydrous DMF was cooled to 0°C on ice bath prior to addition of amine (1 equiv) and Hünig base (2–3 equiv) sequentially to the reaction mixture at 0°C. The reaction mixture was stirred at 0°C and the reaction progress was monitored on an UPLC. The reactions usually completed in 2–3 h. After the completion of reaction, cold water was added to quench the reaction, and the mixture was stirred for 15 min. Mixture was extracted twice with ethyl acetate or dichloromethane, the combined organic layer was washed with 1N HCl, water, saturated NaHCO$_3$ solution and saturated brine solution. Organic layer was further dried over anhydrous Na$_2$SO$_4$ and evaporated under vacuum to give product, which was used directly used in next step without further purification or purified by flash column chromatography or preparative LCMS.

General procedure for Boc-deprotection

The solution of substrate in dichloromethane was cooled to 0°C prior to addition of trifluoroacetic acid (20% v/v with respect to dichloromethane) dropwise at 0°C with stirring. The mixture was allowed to warm to room temperature gradually over a period of 1 h and stirred until the completion of reaction (2–3 h; monitored on an UPLC). Excess trifluoroacetic acid and dichloromethane were evaporated and the residue was dried under vacuum.
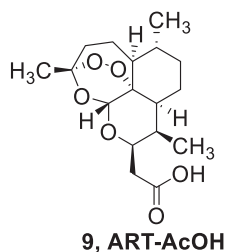

9, ART-AcOH

Preparation of 2-((3R,5aS,6R,8aS,9R,10R,12R,12aR)-3,6,9-trimethyldecahydro-12H-3,12-epoxy[1,2]dioxepino[4,3-i]isochromen-10-yl)acetic acid 9

Using artemisinin as the starting material, ART-AcOH 9 was synthesized in four steps according to the literature procedures.[4] ^{1}H NMR (500 MHz, CDCl$_3$) δ 5.34 (s, 1H), 4.83 (ddd, J = 9.9, 6.0, 3.7 Hz, 1H), 2.75–2.62 (m, 2H), 2.49 (dd, J = 15.6, 3.5 Hz, 1H), 2.31 (td, J = 14.0, 3.7 Hz, 1H), 2.06–1.88 (m, 3H), 1.81–1.75 (m, 1H), 1.70–1.62 (m, 2H), 1.40 (s, 3H), 1.31–1.21 (m, 4H), 0.95 (d, J = 5.9 Hz, 3H), 0.86 (d, J = 7.6 Hz, 3H). ^{13}C NMR (125 MHz, CDCl$_3$) δ 176.45, 103.39, 89.43, 80.95, 71.15, 52.22, 44.03, 37.55, 36.56, 35.94, 34.47, 29.84, 25.93, 24.82, 24.77, 20.21, 12.89. ES$^+$ calc. for C$_{17}$H$_{26}$O$_4$ [M−O$_2$]$^+$: 294.
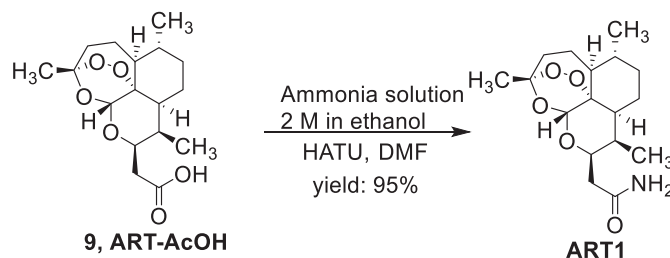
Preparation of 2-((3R,5aS,6R,8aS,9R,10R,12R,12aR)-3,6,9-trimethyldecahydro-12H-3,12-epoxy[1,2]dioxepino[4,3-i]isochromen-10-yl)acetamide ART1

The title compound was synthesized by following the general procedure for HATU mediated coupling of 9 (32.6 mg, 100 μmol) and 2 M Ammonia solution in ethanol (1 mL, 2 mmol). After completion of reaction, mixture was purified by preparative LCMS to give product (31.0 mg, 95%) as a white solid. ^{1}H NMR (500 MHz, CDCl$_3$) δ 6.98 (s, 1H), 5.58 (s, 1H), 5.37 (s, 1H), 4.79 (dd, J = 11.0, 6.1 Hz, 1H), 2.63–2.49 (m, 2H), 2.31 (dt, J = 14.0, 7.3 Hz, 2H), 2.04 (d, J = 14.4 Hz, 2H), 1.96 (dd, J = 10.1, 4.4 Hz, 1H), 1.83–1.62 (m, 3H), 1.37 (s, 3H), 1.31–1.19 (m, 3H), 1.02–0.90 (m, 4H), 0.87 (d, J = 7.5 Hz, 3H). ^{13}C NMR (125 MHz, CDCl$_3$) δ 174.65, 103.06, 90.28, 81.00, 69.79, 51.91, 43.47, 37.64, 37.31, 36.60, 34.34, 30.52, 25.84, 24.93, 24.92, 20.11, 12.11. HRMS calc. for C$_{17}$H$_{27}$NNaO$_5$ [M + Na]$^+$: 348.1781. Found: 348.1770.
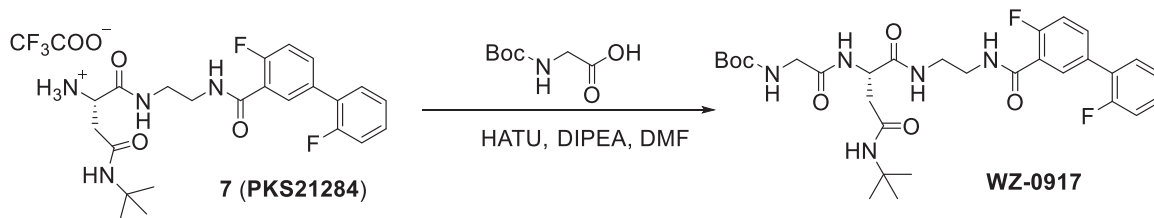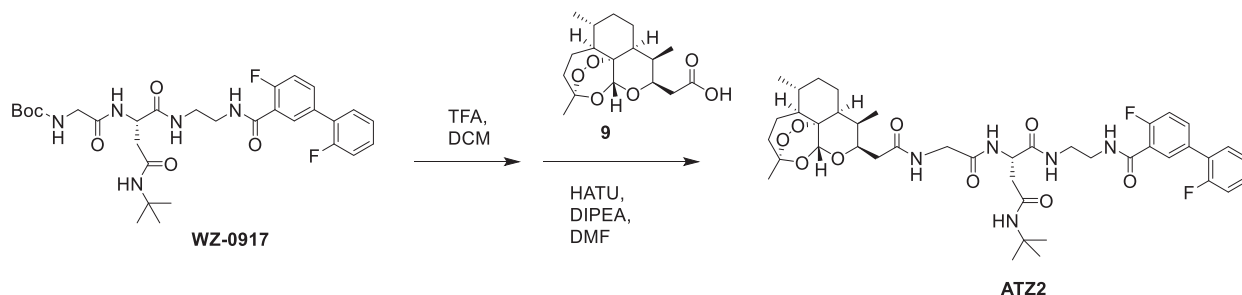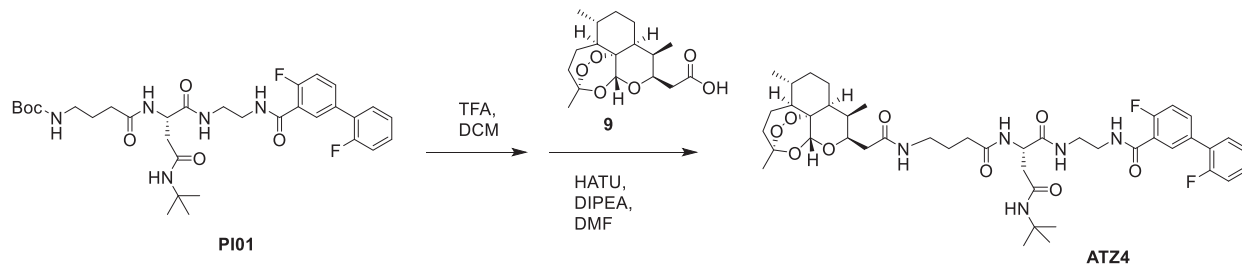

Preparation of tert-butyl (S)-(2-((4-(tert-butylamino)-1-((2-(2′,4-difluoro-[1,1′-biphenyl]-3-carboxamido)ethyl)amino)-1,4-dioxobutan-2-yl)amino)-2-oxoethyl)carbamate WZ-0917

The title compound was synthesized by following the general procedure for HATU mediated coupling of Boc-Gly-OH (19.3 mg, 110 μmol) and 7 (56.0 mg, 100 μmol). After completion of reaction, mixture was purified by preparative LCMS to give product (54.2 mg, 90%) as a white solid. ^{1}H NMR (500 MHz, CDCl$_3$) δ 8.22–7.98 (m, 2H), 7.76 (s, 1H), 7.63–7.47 (m, 2H), 7.40 (dd, J = 11.1, 4.2 Hz, 1H), 7.33–7.27 (m, 1H), 7.20–7.08 (m, 3H), 6.30 (s, 1H), 5.74 (s, 1H), 4.69 (d, J = 6.4 Hz, 1H), 3.74 (qd, J = 17.0, 5.5 Hz, 2H), 3.58 (s, 2H), 3.51–3.32 (m, 2H), 2.78 (dd, J = 14.6, 3.7 Hz, 1H), 2.44 (dd, J = 14.7, 4.8 Hz, 1H), 1.36 (s, 9H), 1.20 (s, 9H). ^{13}C NMR (125 MHz, CDCl$_3$) δ 174.09, 171.76, 170.41, 170.05, 164.30, 163.23, 160.98, 160.64, 158.99, 158.66, 156.75, 133.75, 133.70, 132.49, 132.47, 131.98, 130.69, 130.67, 129.62, 129.56, 127.24, 127.14, 124.62, 124.59, 121.80, 121.70, 116.36, 116.28, 116.16, 116.10, 80.53, 51.50, 50.62, 44.69, 39.98, 39.91, 37.60, 28.52, 28.30. ES$^+$ calc. for C$_{30}$H$_{40}$F$_2$N$_5$O$_6$ [M + H]$^+$: 604.3. Found: 604.3.
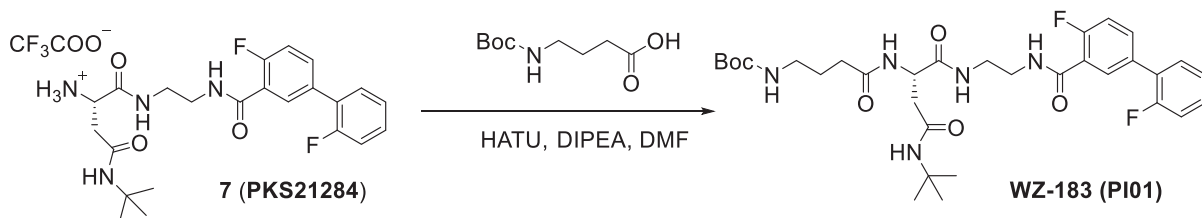
Preparation of tert-butyl (S)-(4-((4-(tert-butylamino)-1-((2-(2′,4-difluoro-[1,1′-biphenyl]-3-carboxamido)ethyl)amino)-1,4-dioxobutan-2-yl)amino)-4-oxobutyl)carbamate PI01

The title compound was synthesized by following the general procedure for HATU mediated coupling of *Boc-GABA-OH* (22.5 mg, 110 μmol) and 7 (56.0 mg, 100 μmol). After completion of reaction, mixture was purified by preparative LCMS to give product (56.2 mg, 89%) as a white solid. ^{1}H NMR (500 MHz, CDCl$_3$) δ 8.14 (d, *J* = 6.2 Hz, 1H), 8.02 (s, 1H), 7.67–7.61 (m, 1H), 7.54 (d, *J* = 6.1 Hz, 1H), 7.44 (t, *J* = 7.3 Hz, 2H), 7.33 (dd, *J* = 13.6, 6.8 Hz, 1H), 7.18 (ddd, *J* = 22.0, 17.3, 9.2 Hz, 3H), 6.01 (s, 1H), 4.71 (s, 2H), 3.68–3.41 (m, 4H), 3.15 (d, *J* = 4.8 Hz, 1H), 2.98 (s, 1H), 2.79 (d, *J* = 13.2 Hz, 1H), 2.46 (d, *J* = 10.0 Hz, 1H), 2.29 (t, *J* = 6.3 Hz, 2H), 1.89 (s, 1H), 1.63 (s, 1H), 1.41 (s, 9H), 1.25 (s, 9H). ^{13}C NMR (125 MHz, CDCl$_3$) δ 172.69, 172.17, 170.89, 164.02, 162.80, 161.10, 160.75, 159.12, 158.78, 156.78, 133.80, 133.76, 132.64, 132.61, 132.28, 130.80, 130.78, 129.70, 129.64, 127.40, 127.29, 124.69, 124.66, 121.88, 121.78, 116.38, 116.20, 79.67, 51.92, 50.77, 40.55, 39.84, 39.04, 38.14, 32.66, 28.60, 28.52, 26.10. HRMS calc. for C$_{32}$H$_{43}$F$_2$N$_5$NaO$_6$ [M + Na]$^+$: 654.3074. Found: 654.3058.

Preparation of (S)-N4-(tert-butyl)-N1-(2-(2′,4-difluoro-[1,1′-biphenyl]-3-carboxamido)ethyl)-2-(2-(2-((3R,5aS,6R,8aS,9R,10R,12R,12aR)-3,6,9-trimethyldecahydro-12H-3,12-epoxy[1,2]dioxepino[4,3-i]isochromen-10-yl)acetamido)acetamido)succinamide ATZ2

The title compound was synthesized by two successive steps, one following the general procedure for Boc-deprotection of WZ-0917 (30.2 mg, 50 μmol) and the other following the general procedure for HATU mediated coupling of 9 (18.0 mg, 55 μmol) with all of the product in first step. After completion of reaction, mixture in the second step was purified by preparative LCMS to give product (33.8 mg, two step yield: 83%) as a white powder. ^{1}H NMR (500 MHz, CDCl$_3$) δ 8.26 (d, *J* = 7.8 Hz, 1H), 8.11 (d, *J* = 5.9 Hz, 1H), 7.85 (t, *J* = 4.7 Hz, 1H), 7.76 (d, *J* = 6.7 Hz, 1H), 7.65–7.56 (m, 2H), 7.44 (t, *J* = 7.4 Hz, 1H), 7.32 (dd, *J* = 12.9, 6.4 Hz, 1H), 7.23–7.10 (m, 3H), 5.89 (s, 1H), 5.37 (s, 1H), 4.85 (dd, *J* = 10.8, 6.1 Hz, 1H), 4.64–4.57 (m, 1H), 3.81 (d, *J* = 5.1 Hz, 2H), 3.69–3.58 (m, 2H), 3.47 (d, *J* = 5.1 Hz, 2H), 2.78 (dd, *J* = 14.7, 3.8 Hz, 1H), 2.60–2.50 (m, 2H), 2.39 (dd, *J* = 14.7, 5.1 Hz, 1H), 2.31 (dd, *J* = 22.6, 9.5 Hz, 2H), 2.06–1.99 (m, 1H), 1.94 (d, *J* = 11.7 Hz, 1H), 1.79–1.71 (m, 1H), 1.71–1.60 (m, 2H), 1.35 (s, 3H), 1.32–1.11 (m, 13H), 1.04–0.87 (m, 4H), 0.80 (d, *J* = 7.4 Hz, 3H). ^{13}C NMR (125 MHz, CDCl$_3$) δ 174.11, 171.41, 170.56, 168.98, 164.08, 164.06, 162.91, 160.99, 160.74, 159.00, 158.77, 133.60, 133.57, 133.53, 133.50, 132.48, 132.46, 132.16, 130.81, 130.79, 129.64, 129.57, 127.40, 127.29, 124.67, 124.64, 122.43, 122.33, 116.35, 116.33, 116.17, 116.13, 103.25, 89.94, 80.93, 70.32, 52.03, 51.68, 50.96, 44.36, 43.64, 40.06, 40.04, 37.57, 37.23, 36.76, 36.55, 34.33, 30.28, 28.55, 25.91, 24.90, 24.85, 20.14, 12.27. HRMS calc. for C$_{42}$H$_{55}$F$_2$N$_5$NaO$_9$ [M + Na]$^+$: 834.3860. Found: 834.3876.

Preparation of (S)-N4-(tert-butyl)-N1-(2-(2′,4-difluoro-[1,1′-biphenyl]-3-carboxamido)ethyl)-2-(4-(2-((3R,5aS,6R,8aS,9R,10R,12R,12aR)-3,6,9-trimethyldecahydro-12H-3,12-epoxy[1,2]dioxepino[4,3-i]isochromen-10-yl)acetamido)butanamido)succinamide ATZ4
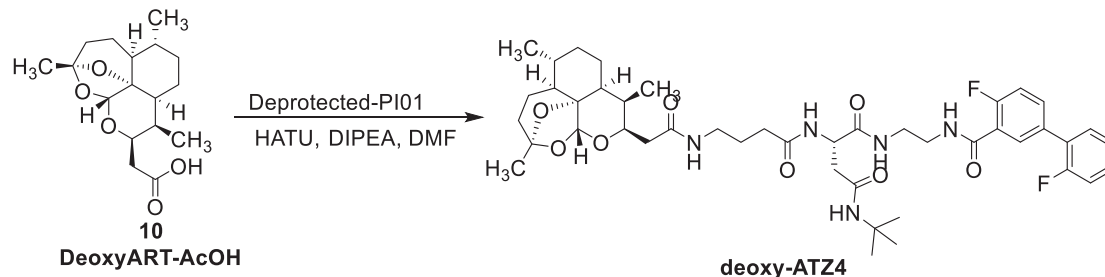
The title compound was synthesized by two successive steps, one following the general procedure for Boc-deprotection of PI01 (31.5 mg, 50 μmol) and the other following the general procedure for HATU mediated coupling of 9 (18.0 mg, 55 μmol) with all of the product in first step. After completion of reaction, mixture in the second step was purified by preparative LCMS to give product

(31.5 mg, two step yield: 75%) as a white powder. ^{1}H NMR (500 MHz, CDCl$_3$) δ 8.13 (d, J = 6.3 Hz, 1H), 8.05 (s, 1H), 7.65 (s, 2H), 7.55–7.48 (m, 1H), 7.43 (t, J = 7.3 Hz, 1H), 7.40–7.30 (m, 2H), 7.24–7.11 (m, 3H), 6.25 (s, 1H), 5.44 (s, 1H), 4.74 (s, 1H), 4.64 (dd, J = 11.0, 6.1 Hz, 1H), 3.63 (d, J = 4.4 Hz, 2H), 3.50 (d, J = 4.5 Hz, 2H), 3.33 (dt, J = 22.8, 11.6 Hz, 1H), 3.09 (dd, J = 12.4, 5.8 Hz, 1H), 2.71 (dd, J = 14.2, 5.2 Hz, 1H), 2.63–2.46 (m, 3H), 2.39–2.25 (m, 4H), 2.03 (t, J = 12.5 Hz, 1H), 1.94 (d, J = 10.9 Hz, 2H), 1.79–1.60 (m, 4H), 1.36 (s, 3H), 1.30–1.11 (m, 13H), 1.00–0.87 (m, 4H), 0.81 (d, J = 7.4 Hz, 3H).^{13}C NMR (125 MHz, CDCl$_3$) δ 173.75, 173.47, 172.24, 170.85, 164.46, 161.05, 160.73, 159.06, 158.76, 134.02, 133.99, 133.94, 133.91, 132.72, 132.69, 132.14, 130.75, 130.72, 129.78, 129.72, 127.23, 127.13, 124.73, 124.70, 121.65, 121.55, 116.46, 116.40, 116.26, 116.22, 103.50, 89.81, 81.00, 70.87, 52.01, 51.92, 50.95, 43.78, 40.02, 38.38, 37.94, 37.60, 36.89, 36.52, 34.33, 32.23, 30.23, 28.53, 25.86, 25.05, 24.93, 24.80, 20.13, 12.43. HRMS calc. for C$_{44}$H$_{59}$F$_2$N$_5$NaO$_9$ [M + Na]$^+$: 862.4173. Found: 862.4147.
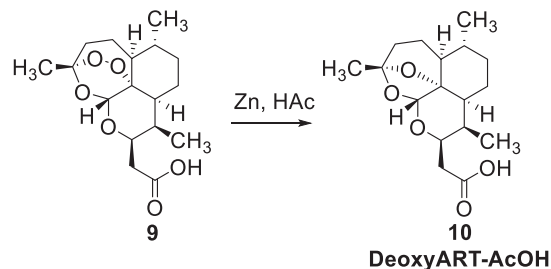

DeoxyART-AcOH 10

The title compound was prepared from *9* by an activated zinc mediated reduction according to the literature procedures.[4] ^{1}H NMR (500 MHz, CDCl$_3$) δ 5.26 (s, 1H), 4.61 (q, J = 7.3 Hz, 1H), 2.57–2.44 (m, 2H), 2.33 (h, J = 8.0 Hz, 1H), 1.96 (ddd, J = 13.1, 8.4, 4.0 Hz, 1H), 1.85 (dt, J = 13.3, 3.8 Hz, 1H), 1.77 (dt, J = 13.1, 3.8 Hz, 1H), 1.73–1.66 (m, 2H), 1.58 (dq, J = 12.8, 5.9 Hz, 2H), 1.25 (q, J = 6.0, 4.9 Hz, 3H), 1.23–1.18 (m, 1H), 1.18–1.12 (m, 2H), 0.99–0.78 (m, 8H). ^{13}C NMR (125 MHz, CDCl$_3$) δ 176.68, 107.56, 97.04, 82.65, 65.76, 45.39, 40.34, 37.31, 35.68, 34.62, 34.55, 29.09, 25.16, 23.69, 22.30, 18.87, 12.45. HRMS calc. for C$_{17}$H$_{26}$NaO$_5$ [M + Na]$^+$: 333.1672. Found: 333.1681.

Preparation of (S)-N4-(tert-butyl)-N1-(2-(2′,4-difluoro-[1,1′-biphenyl]-3-carboxamido)ethyl)-2-(4-(2-((2R,3R,3aS,3a1R,6R,6aS,9S,10aR)-3,6,9-trimethyldecahydro-10aH-3a1,9-epoxyoxepino [4,3,2-ij]isochromen-2-yl)acetamido)butanamido)succinamide Deoxy-ATZ4
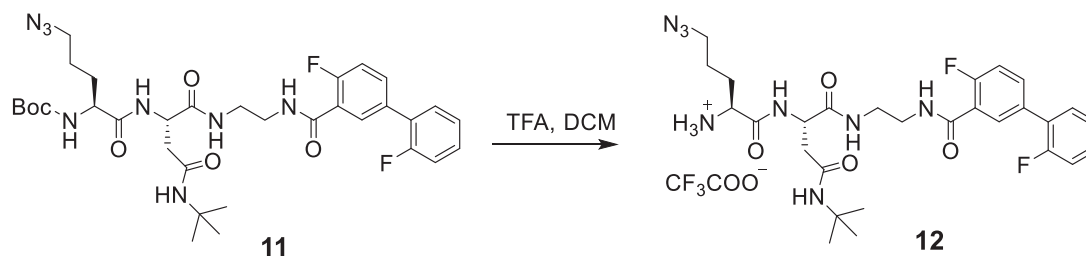
The title compound was synthesized by two successive steps, one following the general procedure for Boc-deprotection of PI01 (15.7 mg, 25 μmol) and the other following the general procedure for HATU mediated coupling of *10* (9.3 mg, 30 μmol) with all of the product in first step. After completion of reaction, mixture in the second step was purified by preparative LCMS to give product (18.0 mg, two step yield: 89%) as a white powder. ^{1}H NMR (500 MHz, CDCl$_3$) δ 8.17–8.09 (m, 2H), 7.63 (tq, J = 4.5, 3.0, 2.2 Hz, 2H), 7.45 (td, J = 7.8, 1.8 Hz, 1H), 7.38–7.29 (m, 1H), 7.32–7.27 (m, 1H), 7.21 (td, J = 7.5, 1.3 Hz, 1H), 7.19–7.10 (m, 2H), 6.64 (dd, J = 8.6, 4.4 Hz, 1H), 5.77 (s, 1H), 5.27 (s, 1H), 4.80 (dt, J = 8.2, 5.1 Hz, 1H), 4.43 (ddd, J = 10.4, 7.1, 2.7 Hz, 1H), 3.63 (q, J = 5.3 Hz, 2H), 3.57–3.46 (m, 3H), 2.89 (dq, J = 13.8, 4.5 Hz, 1H), 2.72 (dd, J = 14.9, 5.1 Hz, 1H), 2.51 (dd, J = 14.9, 5.3 Hz, 1H), 2.28–2.10 (m, 5H), 2.08–1.82 (m, 3H), 1.81–1.66 (m, 2H), 1.64–1.51 (m, 1H), 1.25 (s, 10H), 1.23–1.10 (m, 4H), 0.96 (td, J = 12.4, 11.5, 3.2 Hz, 1H), 0.89 (d, J = 5.6 Hz, 3H), 0.76 (d, J = 7.6 Hz, 3H). ^{13}C NMR (125 MHz, CDCl$_3$) δ 172.72, 172.50, 172.02, 170.69, 170.58, 163.94, 163.92, 160.98, 160.77, 158.99, 158.80, 133.52, 133.49, 133.45, 133.41, 132.50, 132.48, 132.16, 132.14, 132.12, 130.84, 130.82, 129.65, 129.59, 127.44, 127.34, 124.68, 124.65, 122.62, 122.51, 116.37, 116.31, 116.19, 116.12, 107.88, 97.25, 82.64, 65.70, 51.57, 50.50, 45.28, 40.31,

40.00, 39.72, 38.78, 38.39, 37.31, 35.73, 34.55, 34.50, 32.28, 29.54, 28.69, 28.66, 26.11, 25.30, 23.77, 22.26, 18.87, 12.03. HRMS calc. for $C_{44}H_{60}F_2N_5O_8$ [M + H]$^+$: 824.4404. Found: 824.4435.
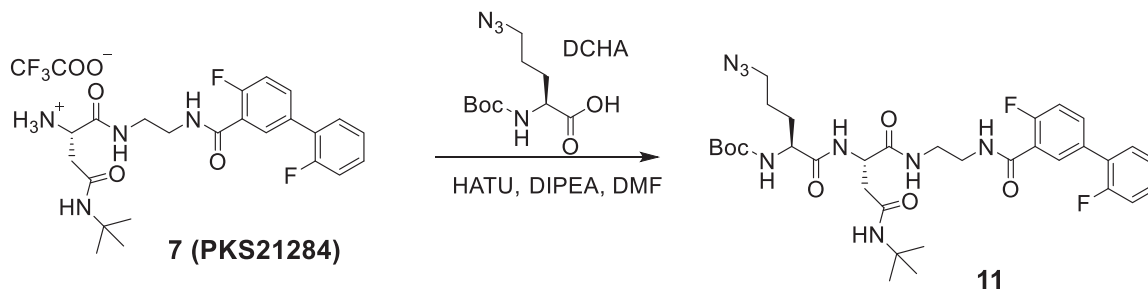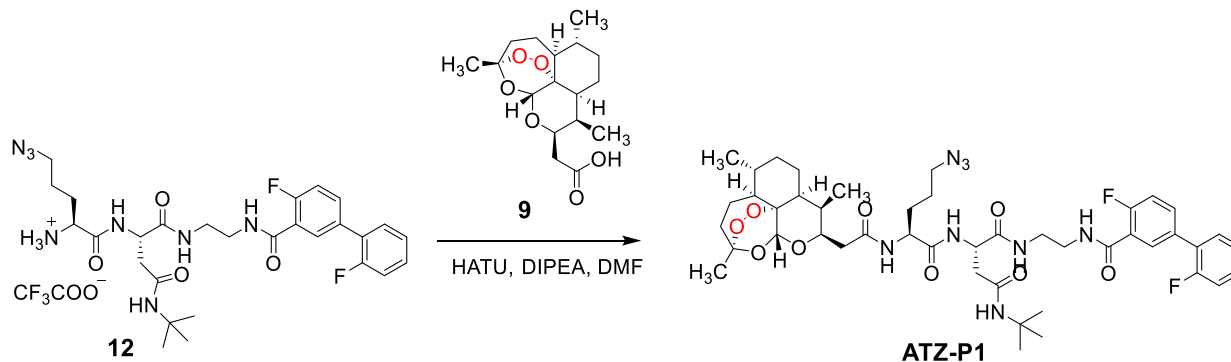

Preparation of tert-butyl ((S)-5-azido-1-(((S)-4-(tert-butylamino)-1-((2-(2′,4-difluoro-[1,1′-biphenyl]-3-carboxamido)ethyl)amino)-1,4-dioxobutan-2-yl)amino)-1-oxopentan-2-yl)carbamate 11

The title compound was synthesized by following the general procedure for HATU mediated coupling of (S)-5-azido-2-((tert-butoxycarbonyl)amino)pentanoic acid dicyclohexylamine salt (440.0 mg, 1.0 mmol) and 7 (560.0 mg, 1.0 mmol). After completion of reaction, the mixture was purified by flash column chromatography to give the title product (550.0 mg, 80%) as a white solid. ^{1}H NMR (500 MHz, DMSO-d_6) δ 8.34 (t, J = 5.3 Hz, 1H), 8.05 (t, J = 8.8 Hz, 1H), 7.85 (d, J = 5.8 Hz, 1H), 7.79 (d, J = 6.7 Hz, 1H), 7.73–7.66 (m, 1H), 7.56 (t, J = 8.0 Hz, 1H), 7.49–7.28 (m, 6H), 7.05 (d, J = 7.2 Hz, 1H), 4.41 (q, J = 7.0 Hz, 1H), 3.86 (q, J = 6.7, 6.2 Hz, 1H), 3.39–3.24 (m, 6H), 3.20–3.06 (m, 2H), 2.89 (s, 1H), 2.73 (s, 1H), 2.69 (d, J = 1.5 Hz, 2H), 2.43 (h, J = 7.3, 6.0 Hz, 2H), 1.97 (d, J = 11.0 Hz, 1H), 1.75 (d, J = 11.8 Hz, 1H), 1.63 (td, J = 13.3, 12.7, 5.0 Hz, 2H), 1.52 (p, J = 7.6, 6.2 Hz, 4H), 1.38 (s, 9H), 1.31–1.19 (m, 4H), 1.18 (s, 9H). ^{13}C NMR (125 MHz, DMSO) δ 171.42, 170.89, 168.97, 168.51, 164.58, 163.43, 162.29, 159.96, 159.80, 158.00, 157.80, 155.62, 132.71, 132.68, 132.63, 132.61, 131.30, 131.27, 130.77, 130.74, 130.36, 130.33, 130.31, 129.99, 129.93, 126.67, 126.57, 125.02, 124.99, 124.21, 124.10, 116.56, 116.38, 116.22, 116.04, 78.41, 55.04, 54.88, 54.07, 52.22, 50.39, 50.33, 50.14, 50.05, 49.95, 48.58, 38.91, 38.38, 38.22, 37.99, 36.49, 35.76, 35.21, 30.75, 28.91, 28.83, 28.45, 28.36, 28.15, 24.83, 24.75, 23.85. ES$^+$ calc. for $C_{33}H_{45}F_2N_8O_6$ [M + H]$^+$: 687.3. Found 687.5.
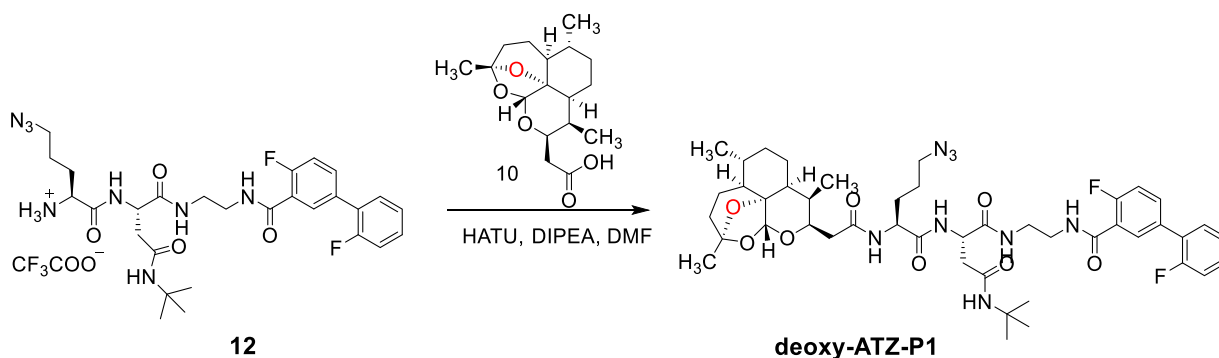

Preparation of (S)-2-((S)-2-amino-5-azidopentanamido)-N^4-(tert-butyl)-N^1-(2-(2′,4-difluoro-[1,1′-biphenyl]-3-carboxamido)ethyl)succinamide trifluoroacetate salt 12

The title compound was synthesized by following the general procedure for Boc-deprotection of 11 (343.0 mg, 500 μmol). The isolated colorless gum (350.0 mg, quant.) was used in next step without further purification. ES$^+$ calc. for $C_{28}H_{37}F_2N_8O_4$ [M + H]$^+$: 587.3. Found 587.5.

Preparation of (S)-2-((S)-5-azido-2-(2-((3R,5aS,6R,8aS,9R,10R,12R,12aR)-3,6,9-trimethyldecahydro-12H-3,12-epoxy[1,2]dioxepino[4,3-i]isochromen-10-yl)acetamido)pentanamido)-N[4]-(tert-butyl)-N[1]-(2-(2′,4-difluoro-[1,1′-biphenyl]-3-carboxamido)ethyl)succinimide ATZ-P1

The title compound was synthesized by following the general procedure for HATU mediated coupling of 9 (45.0 mg, 138 μmol) and 12 (105.0 mg, 150 μmol). After completion of reaction, mixture was purified by preparative LCMS to give product (94.0 mg, 76%) as a white powder. ^{1}H NMR (500 MHz, CDCl$_3$) δ 8.64 (d, J = 7.5 Hz, 1H), 8.09 (dd, J = 7.2, 2.3 Hz, 1H), 8.04 (d, J = 4.6 Hz, 1H), 7.87–7.76 (m, 1H), 7.62 (ddd, J = 8.4, 4.4, 2.1 Hz, 1H), 7.50 (t, J = 5.5 Hz, 1H), 7.44 (t, J = 7.7 Hz, 1H), 7.33 (q, J = 6.7 Hz, 1H), 7.26 (s, 1H), 7.21 (t, J = 7.5 Hz, 1H), 7.14 (ddd, J = 10.7, 8.7, 5.0 Hz, 2H), 5.66 (s, 1H), 5.39 (s, 1H), 5.02 (dd, J = 11.9, 6.3 Hz, 1H), 4.48 (dt, J = 8.2, 4.3 Hz, 1H), 4.04 (dt, J = 9.0, 4.5 Hz, 1H), 3.64 (qt, J = 14.1, 7.0 Hz, 2H), 3.48 (q, J = 5.4 Hz, 2H), 3.30 (hept, J = 6.5 Hz, 2H), 2.76–2.68 (m, 1H), 2.68–2.59 (m, 1H), 2.55 (dd, J = 17.2, 12.0 Hz, 1H), 2.33 (td, J = 14.6, 13.7, 7.7 Hz, 3H), 2.09–2.01 (m, 2H), 2.01–1.91 (m, 2H), 1.72 (dddd, J = 37.8, 17.5, 12.9, 4.5 Hz, 7H), 1.39 (s, 4H), 1.26 (td, J = 10.4, 9.0, 4.1 Hz, 6H), 1.21 (s, 9H), 0.96 (t, J = 7.1 Hz, 5H), 0.82 (d, J = 7.5 Hz, 3H). ^{13}C NMR (125 MHz, CDCl$_3$) δ 173.99, 171.07, 170.89, 170.23, 163.85, 163.83, 160.82, 160.62, 158.82, 158.65, 133.29, 133.25, 133.22, 133.18, 132.26, 132.24, 132.07, 132.05, 132.03, 130.71, 130.69, 129.48, 129.42, 127.33, 127.22, 124.53, 124.50, 122.69, 122.59, 116.21, 116.11, 116.03, 115.92, 103.40, 89.66, 80.62, 70.08, 55.00, 51.96, 51.62, 51.28, 50.97, 43.78, 40.04, 37.50, 36.83, 36.43, 36.13, 34.23, 29.94, 28.36, 28.12, 25.91, 25.77, 24.87, 24.73, 24.67, 20.03, 12.36. HRMS calc. for C$_{45}$H$_{61}$F$_2$N$_8$O$_9$ [M + H]$^+$: 895.4524. Found: 895.4560.

12   **10**   HATU, DIPEA, DMF   **deoxy-ATZ-P1**

Preparation of (S)-2-((S)-5-azido-2-(2-((2R,3R,3aS,3a^{1}R,6R,6aS,9S,10aR)-3,6,9-trimethyldecahydro-10aH-3a^1,9-epoxyoxepino[4,3,2-ij]isochromen-2-yl)acetamido)pentanamido)-N[4]-(tert-butyl)-N[1]-(2-(2′,4-difluoro-[1,1′-biphenyl]-3-carboxamido)ethyl)succinamide deoxy-ATZ-P1

The title compound was synthesized by following the general procedure for HATU mediated coupling of 10 (40.0 mg, 130 μmol) and 12 (105.0 mg, 150 μmol). After completion of reaction, mixture was purified by preparative LCMS to give product (91.0 mg, 80%) as a white powder. ^{1}H NMR (500 MHz, CDCl$_3$) δ 8.76 (d, J = 7.3 Hz, 1H), 8.08 (dd, J = 7.1, 2.3 Hz, 1H), 7.91 (q, J = 6.0 Hz, 1H), 7.65–7.58 (m, 1H), 7.55 (t, J = 5.4 Hz, 1H), 7.51 (d, J = 4.2 Hz, 1H), 7.43 (td, J = 7.8, 1.7 Hz, 1H), 7.36–7.28 (m, 1H), 7.20 (t, J = 7.5 Hz, 1H), 7.14 (ddd, J = 12.6, 8.5, 4.5 Hz, 2H), 5.97 (s, 1H), 5.33 (s, 1H), 4.83 (td, J = 8.9, 8.0, 4.1 Hz, 1H), 4.47 (dt, J = 8.0, 4.4 Hz, 1H), 4.01 (p, J = 4.0 Hz, 1H), 3.67 (t, J = 9.5 Hz, 1H), 3.62 (s, 1H), 3.46 (ddt, J = 13.9, 9.3, 4.5 Hz, 2H), 3.28 (t, J = 6.4 Hz, 2H), 2.74 (dd, J = 14.5, 3.8 Hz, 1H), 2.40–2.32 (m, 2H), 2.27 (td, J = 16.2, 15.1, 6.2 Hz, 2H), 1.98 (dt, J = 13.2, 4.0 Hz, 1H), 1.97–1.91 (m, 1H), 1.91–1.84 (m, 1H), 1.83–1.76 (m, 1H), 1.74 (dt, J = 8.9, 4.2 Hz, 4H), 1.69 (d, J = 5.1 Hz, 1H), 1.53 (s, 3H), 1.28–1.19 (m, 1H), 1.19 (s, 9H), 0.96 (dt, J = 13.9, 10.5 Hz, 1H), 0.90 (d, J = 5.3 Hz, 3H), 0.78 (d, J = 7.5 Hz, 3H). ^{13}C NMR (125 MHz, CDCl$_3$) δ 174.49, 171.15, 170.96, 170.45, 163.91, 163.89, 162.74, 160.78, 160.62, 158.78, 158.65, 133.37, 133.33, 133.30, 133.26, 132.28, 132.25, 132.05, 132.03, 132.01, 130.70, 130.68, 129.47, 129.41, 127.32, 127.22, 124.51, 124.48, 122.60, 122.50, 116.23, 116.14, 116.05, 115.94, 108.08, 97.24, 82.55, 64.76, 55.19, 51.61, 51.35, 50.98, 45.13, 39.95, 39.90, 39.79, 37.64, 36.63, 35.59, 34.41, 29.30, 28.35, 28.12, 25.60, 25.21, 23.17, 22.08, 18.72, 11.78. HRMS calc. for C$_{45}$H$_{61}$F$_2$N$_8$O$_8$ [M + H]$^+$: 879.4575. Found: 879.4599.

QUANTIFICATION AND STATISTICAL ANALYSIS

All enzyme inhibition and cell viability assays were done in duplicates or triplicates as indicated in the figure legends, and the data are presented as mean ± SD or SEM. All data fitting and statistical analysis was performed using GraphPad Prism software (Version 9.4.0).